https://doi.org/10.1016/j.envpol.2020.116163

Impact of weather and emission changes on NO_2 concentrations in China during 2014−2019

Yang Shen [a], Fei Jiang [a,b*], Shuzhuang Feng [a], Yanhua Zheng [a], Zhe Cai [c], Xiaopu Lyu [d]

[a] *Jiangsu Provincial Key Laboratory of Geographic Information Science and Technology, International Institute for Earth System Science, Nanjing University, Nanjing, 210023, China*

[b] *Jiangsu Center for Collaborative Innovation in Geographical Information Resource Development and Application, Nanjing, 210023, China*

[c] *Nanjing Climblue Technology co., LTD, Nanjing, Jiangsu 211135, China*

[d] *Department of Civil and Environmental Engineering, Hong Kong Polytechnic University, Hong Kong*

* Corresponding author

E-mail address: jiangf@nju.edu.cn; Tel.: +86-25-89687077; Fax: +86-25-89682288;

Abstract: Nitrogen dioxide (NO_2) is one of the most important air pollutants that highly affect the formation of secondary fine particles and tropospheric ozone. In this study based on hourly NO_2 observations from June 2014 to May 2019 and a regional air quality model (WRF−CMAQ), we comprehensively analyzed the spatiotemporal variations of NO_2 concentrations throughout China and in 12 urban agglomerations (UAs) and quantitatively showed the anthropogenic and meteorological factors controlling the interannual variations (IAVs). The ground observations and tropospheric columns show that high NO_2 concentrations are predominantly concentrated in UAs such as Beijing−Tianjin−Hebei (BTH), the Shandong Peninsula (SP), the Central Plain (CP), Central Shaanxi (CS), and the Yangtze River Delta (YRD). For different UAs, the NO_2 IAVs are different. The NO_2 increased first and then decreased in 2016 or 2017 in BTH, YRD, CS, and Cheng−Yu, and decreased from 2014 to 2019 in Harbin−Changchun, CP, SP, Northern Slope of Tianshan Mountain, and Beibu−Gulf,

while increased slightly in the Pearl River Delta (PRD) and Hohhot−Baotou−Erdos−Yulin (HBEY). The NO_2 IAVs were primarily dominated by emission changes. The net wintertime decreases of NO_2 in BTH, Yangtze River Middle−Reach, and PRD were mostly contributed by emission reductions from 2014 to 2018, and the significant increase in the wintertime in HBEY was also dominated by emission changes (93%). Weather conditions also have an important effect on the NO_2 IAVS. In BTH and HBEY, the increases of NO_2 in winter of 2016 are mainly attributed to the unfavorable weather conditions and for the significant decreases in the winter of 2017, the favorable weather conditions also play a very important role. This study provides a basic understanding on the current situation of NO_2 pollution and are helpful for policymakers as well as those interested in the study of tropospheric ozone changes in China and downwind areas.

Keywords: NO_2; urban agglomeration; spatiotemporal pattern; WRF−CMAQ; quantitative impacts

Capsule: This study quantitatively separated the anthropogenic and meteorological contributions related to the NO_2 interannual variations.

1. Introduction

The severe air pollution in China from accelerated urbanization has received widespread attention. Under the implementation of increasingly stringent and the toughest-ever clean air policies and legislations, the concentrations of fine particulate matter ($PM_{2.5}$) decreased significantly in recent years in typical urban agglomerations (UAs) in China (Zhang et al., 2019a; Zhang et al., 2019b; Fan et al., 2020a). Nitrogen dioxide (NO_2) is a primary gaseous pollutant that play an important role in atmospheric chemistry and human health (Tiwari et al., 2015; Sun et al., 2019a). NO_2 is a major precursor of both secondary $PM_{2.5}$ and ozone formations and is related to a series of environmental problems (Xie et al., 2009; Carmona-Cabezas et al., 2020). Additionally,

NO_2 also causes various diseases and is associated with the mortality of pulmonary heart disease (Chen et al., 2019a), lung function impairment (Jiang et al., 2019), depression (Fan et al., 2020b), and changes in blood lipid levels (Mao et al., 2020).

The spatiotemporal patterns of NO_2 pollution were widely studied based on satellite NO_2 retrievals from the Ozone Monitoring Instrument (OMI) for the large-scale, high-spatial resolution and global coverage of the data (Xie et al., 2018; Silvern et al., 2019). The trend and spatial distribution of tropospheric NO_2 columns in some areas of China, such as Henan Province, the Inner Mongolia region and the Sichuan Basin, were analyzed using OMI retrievals (Zhang et al., 2017; Zheng et al., 2018a; Ai et al., 2018). The most evident decline of NO_2, which occurred at a rate of $-7.3 \pm 1.5\%$ per year from 2012 to 2017, was detected in eastern China by tropospheric NO_2 column analysis (Lin et al., 2019). Although satellite measurements can explain integrant spatial variability, they still presented some uncertainties (Just et al., 2015), therefore, many studies on the spatial and temporal variations of NO_2 based on ground observations were also conducted worldwide (Chai et al., 2014; Chen et al., 2015; Li et al., 2017a; Ielpo et al., 2019; Hunova et al., 2020). For example, Kasparoglu et al. (2018) reported the first continuous records of NO_2 concentrations, nitric oxide, and surface ozone at both rural and urban air quality sites in the Marmara region of Turkey. Studies on NO_2 characteristics in China are primarily focused on the mega cities like Beijing, Shanghai, Guangzhou, Chengdu, and Hong Kong (Xu et al., 2019a; Liu et al., 2016; Wu et al., 2019; Shi et al., 2018; Anand and Monks, 2017); UAs such as the Beijing−Tianjin−Hebei (BTH), the Yangtze River Delta (YRD), the Pearl River Delta (PRD), and Hohhut−Baotou−Ordos region (Meng et al., 2018; Ma et al., 2019; Xie et al., 2019; Zheng et al., 2018a); and hot spots such as eastern China and the Sichuan Basin (Liu et al., 2018; Zhao et al., 2018). For example, the investigation conducted by Zhou et al. (2018) indicated that the concentrations of surface NO_2 presented an upward trend from 2013−2016 in Lanzhou, a provincial capital city in China. Both OMI-retrieved and surface NO_2 data were used by Xie et al. (2018), and good consistency

was found between the two types of data in the Wanjiang City Belt in Anhui Province along the Yangtze River.

In addition to the characteristics and variations of the spatiotemporal distribution of NO_2, the drivers of the variations are also an important scientific issue. Meteorological conditions are generally primary drivers and can affect the environmental air pollution in many ways (Li et al., 2016; Yang et al., 2016; Zheng et al., 2017; Li et al., 2019; Sun et al., 2019b; Chen et al., 2020). Studies showed that higher NO_2 concentrations are generally associated with lower planetary boundary layer height (PBLH), weaker wind speeds, lower temperature, and higher relative humidity (Zhang et al., 2015; Yang et al., 2020). Additionally, NO_2 is primarily released by anthropogenic emissions and is considered an indicator of combustion sources, such as motor vehicle emissions in urban areas (Wheeler et al., 2008; Shi et al., 2018; Jin et al., 2019). He et al. (2017a) analyzed two-years ground observations of six pollutants in China's 31 provincial capital cities and found that the air quality improvements in 2015 primarily benefited from emissions reduction, because the meteorological conditions in 2015 were not conducive to pollutant diffusion compared to those of 2014. Yang et al. (2019) used the Weather Research and Forecasting with Chemistry (WRF−Chem) model to evaluate the air pollution emission control strategies in western China; results indicated that the reductions of industrial and transportation emissions are essential for reducing SO_2 and NO_2. Fan et al. (2020a) provided the spatio-temporal characteristics of air pollution over China and analyzed the influences of emission control policies on air pollutant variation. However, the analysis was qualitative and did not provide detailed meteorological conditions.

In this study, based on five-year (June 2014 to May 2019) officially released NO_2 data and the tropospheric NO_2 columns (XNO_2) retrieved from the OMI satellite data, we comprehensively analyzed the characteristics of spatiotemporal distributions and the variations of NO_2 concentrations in China and in 12 UAs in recent years. We also used the Weather Research and Forecasting model (WRF) and Community Multiscale

Air Quality (CMAQ) model to quantitatively study the drivers of interannual NO_2 variations. This paper is organized as follows: Section 2 briefly describes the study areas, data, and the air quality model; Section 3 presents the results and discussions, and Section 4 gives the conclusions.

2. Materials and methods

2.1. Study areas

The study area includes all of mainland China (except for Hong Kong, Macau, and Taiwan) and focuses on five national UAs, six regional medium-sized UAs and one sub-regional UA (Figure 1). The UAs were selected according to the "5 + 9 + 6" spatial organization pattern of Chinese UAs (Fang et al., 2018). The five national UAs are BTH, YRD, PRD, the Yangtze River Middle−Reach (YRMR), and Cheng−Yu (CY). The six medium−sized regional UAs are Harbin−Changchun (HC), the Shandong Peninsula (SP), the Central Plains (CP), Central Shaanxi (CS), the Beibu Gulf (BG), and the Northern Slope of Tianshan Mountain (NSTM). The sub−regional UA is Hohhot−Baotou−Erdos−Yulin (HBEY). The acronym and the population and GDP of each typical UA are listed in Table 1.

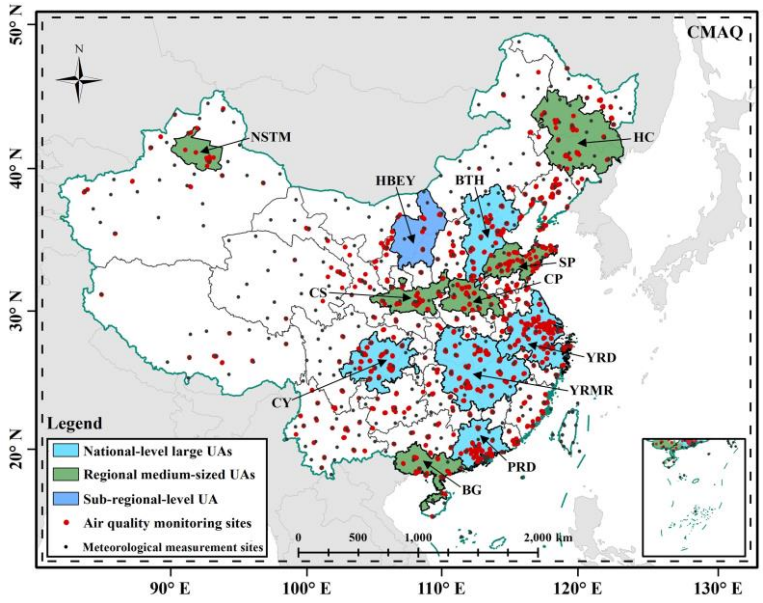

Figure 1. Locations of the 12 UAs, the national air quality monitoring sites (the red

dots) and the meteorological measurement sites (the black dots). The black dashed frame depicts the CMAQ computational domain.

Table 1. Population and GDP of selected UAs [a]

UA	Acronym of UA	Permanent population (million)	GDP (trillion yuan)
Beijing−Tianjin−Hebei [2]	BTH	110.00	7.46
Yangtze River Delta [2]	YRD	150.00	12.67
Yangtze River Middle−Reach [2]	YRMR	121.00	6.00
Cheng−Yu [2]	CY	91.00	3.76
Pearl River Delta [4]	PRD	57.20	6.78
Harbin−Changchun [1]	HC	39.00	2.16
Central Shaanxi [5]	CS	38.65	2.16
Central Plains [5]	CP	78.62	3.45
Shandong Peninsula [3]	SP	67.48	5.09
Northern Slope of Tianshan	NSTM	4.58	0.22
Beibu Gulf [3]	BG	41.41	1.63
Hohhot−Baotou−Erdos−Yulin [4]	HBEY	11.38	1.42

[a] Data were drawn from the China City Statistical Yearbook. The superscripts of 1, 2, 3, 4 and 5 indicate that the statistical year of population and GDP is 2013, 2014, 2015, 2016 and 2017, respectively.

Details of the five national UAs, and the regional medium−sized UAs of HC, CS and NSTM can be found in Shen et al. (2019). SP is the focus of economic and urban development in Shandong province (Zhao and Shu, 2019) and one of the fastest-growing UAs in China's economy and society. CP is an important energy and equipment industry base in central and western China (Duan et al., 2017) and is the hub and core area for industrial transfer between developed countries and the eastern part of China. BG, located in the northwestern part of the South China Sea, is a semi closed bay surrounded by the land on three sides. The key industries are primarily traditional with high energy consumption and emissions that inevitably increase various atmospheric pollutants in the Beibu Gulf area (Hu and Li, 2016). HBEY is an important heavy

chemical industry area with a relatively high level of resource consumption and environmental impacts; thermal power, mining, and metallurgy have significant impacts on air quality (Li et al., 2020a).

2.2. Data

2.2.1. Measurement data

Hourly NO_2 observations from June 2014 to May 2019 were collected from the China National Environmental Monitoring Platform (http://106.37.208.233:20035/). All observations were measured by the chemiluminescence and differential optical absorption spectroscopy methods at monitoring sites with the height of sampling port from the ground within 3-20 meters (MEP, 2009, 2012, 2013). These monitoring sites situated in all prefecture-level cities are presented in Figure 1. Before using these data, the hourly observations that equal to zero were removed, the rest data were averaged to daily, monthly, seasonal and annual concentrations of each city and each UA using the arithmetic mean method. During the calculating of daily and monthly concentrations, based on the requirements of the statistical validity of data stated in GB3095−2012 (MEP, 2012), for each site, the daily NO_2 averages were calculated only when there are at least 20 hours valid data, and the monthly means were calculated when there are at least 27 days valid data per month (at least 25 days in February). Since September 1, 2018, NO_2 measurement was changed from a standard temperature and pressure (STP) state (i.e., atmospheric temperature: 273 K, atmospheric pressure: 1013.25 hPa) to a reference state (i.e., atmospheric temperature: 298.15 K, atmospheric pressure: 1013.25 hPa) (MEP, 2018). In order to guarantee consistency, all the data were converted to STP state concentrations. Table S1 in the Supplementary material shows the number of monitoring sites selected after data quality control in each UA.

2.2.2. OMI XNO_2 retrieval

Satellite XNO_2 retrievals were widely used to investigate the temporal and spatial

variations of NO_2 concentrations and estimate the nitrogen oxides (NO_x) emissions changes over China and the other regions around the world (e.g., Castellanos and Boersma, 2012; Liu et al., 2017a; Bauwens et al., 2020). To investigate whether the temporal and spatial variations of satellite XNO_2 are consistent with those of the ground observations over different UAs in China in recent years, the XNO_2 retrieved from the OMI satellite observations (Boersma et al., 2018) were obtained and compared with the ground observations. The OMI, which provides chemical information on atmospheric trace gases, is located on the NASA Earth Observation System Aura satellite, which overpasses at approximately 13:45 mean local solar time (Levelt et al., 2006). The OMI NO_2 monthly mean data with the spatial resolution of 0.125° × 0.125° (QA4ECV version 1.1, Boersma et al., 2017) were obtained from the website of the Royal Netherlands Meteorological Institute (http://www.temis.nl/airpollution/no2.html). There will be no values or somewhat a higher frequency of negative values in regions that are cloudy or snow-covered (Bucsela et al., 2013). The affected pixels have been removed in this product. The monthly data given are the results of averaging and gridding mostly-clear retrievals, with the associated uncertainties cancelling out or being smoothed when averaging over multiple pixels (spatially) or over time (Boersma et al., 2018).

2.3. Air quality model and configurations

The WRF model (version 3.6) and the CMAQ model (version 5.0.2) were applied to simulate NO_2 concentrations (Skamarock, 2008; Binkowski and Roselle, 2003). The simulation periods were June, July, August (summer), and December of each year from 2014 to 2018, and January and February (winter) of each year from 2015 to 2019, a total of 30 months. The WRF domain covers most areas of East Asia and the horizontal grid resolution is 36 km × 36 km. There is a total of 51 vertical layers and the top of the model is fixed at 50 hPa. The configuration of the CMAQ domain is the same as that of the WRF model, except for three grid cells cut from each side of the WRF domain.

The CMAQ has 15 sigma layers in vertical that were extracted from the WRF model. More details about physical and chemical configurations can be found in Feng et al. (2018).

The Final (FNL) Operational Global Analysis data from the National Center for Environmental Prediction (NCEP) were utilized for lateral boundary conditions and initial conditions of meteorological fields with a resolution of 1° × 1° at a 6−h interval. In mainland China, the anthropogenic emissions were obtained from the Multi-resolution Emission Inventory of China in 2012 (MEIC 2012) (Zheng et al., 2018b); outside mainland China, the anthropogenic emissions were derived from the mosaic Asian anthropogenic emission inventory (MIX) (Li et al., 2017b). Additionally, biogenic emissions were calculated by using the Model of Emissions of Gases and Aerosols from Nature (MEGAN) (Guenther, 2012).

2.4. Method

In this study, WRF−CMAQ runs were conducted with fixed anthropogenic emissions (MEIC 2012) and monthly variational meteorological conditions from 2014 to 2019. The WRF simulation was run continuously for each month, and grid-nudging was applied to stabilize results. These fixed-emission and varied-meteorology simulations provide NO_2 variation contributions from the meteorological condition changes (Xu et al., 2020), enabling the quantification of the yearly meteorological impact. Emission-related NO_2 variations can be derived by subtracting meteorology-related NO_2 variations from observed variations (Liu et al., 2017b; Zhang et al., 2019a).

3. Results and discussions

3.1. Spatial distributions of NO_2 concentrations

3.1.1. Spatial patterns of annual mean NO_2 concentrations

Figure 2a shows the four-year mean spatial distribution of surface NO_2

concentrations in China from 2015 to 2018. The high values of NO_2 concentrations are primarily distributed in the UAs of BTH, western SP, northern CP, central CS, eastern YRD, and some cities in PRD, CY, NSTM, HBEY, and HC; this is similar to the spatial distribution of $PM_{2.5}$ concentrations (Shen et al., 2019). The distributions are basically the same for different years (annual average concentrations maps of surface NO_2 from 2015 to 2018 presented in Figure S1). The OMI XNO_2 retrieval shows a spatial distribution similar to that of ground observations (Figure 2b and Figure S2). Figure 3 shows the mean annual surface NO_2 concentrations of each UA from 2015−2018. BTH, YRD, and CP have the highest NO_2 concentrations, followed by SP, HBEY, and CS. HC, YRMR, and BG have the lowest concentrations—below the national average. Overall, these distributions across UAs are primarily related to NO_x emissions (Figure 3); the areas with high NO_2 values generally have high NO_x emissions, and vice versa. Due to the short lifetime in the atmosphere, the areas with high NO_2 concentrations are usually close to the places with strong NO_x emissions (Lamsal et al., 2013, Feng et al., 2019a, Zhao et al., 2019). Moreover, weather condition is another factor that highly affects the NO_2 concentrations. Usually, strong wind, high temperature, strong radiation and heavy rainfall will result in a low NO_2 concentration (Harkey et al., 2015). The stronger wind is conducive to the transport and diffusion of air pollutants, higher temperature causes faster atmospheric reactions and a higher boundary layer (better vertical mixing), stronger radiation brings faster photolysis, and more rainfall leads to more wet deposition. It could be found that the differences of NO_x emissions among different UAs are more significant than those of NO_2 concentrations. Some UAs have relatively higher NO_x emissions but relatively lower NO_2 concentrations. For example, the emissions of YRD and SP are higher than those of BTH and CP, but the NO_2 concentrations of the former are much lower, primarily because they are located in coastal areas, which have better diffusion conditions than the inland locations (i.e., BTH and CP). Additionally, YRD and SP are located in the transition regions of north and south China and, therefore, have more rainfall than BTH and CP (Li et al., 2020b),

which may cause more wet deposition and lead to lower concentrations. Similarly, PRD has much higher emissions but lower concentrations than HBEY, CS, and NSTM. In addition, HC and YRMR have similar NO_2 concentrations, area, and discrete cities, but HC has much weaker emissions than YRMR. HC is located in Northeast China, while YRMR is located in Central China, indicating that HC has much weaker radiation and lower temperature than YRMR, resulting in higher NO_2 concentrations per unit NO_x emitted in HC (Chen et al., 2019b; Yang et al., 2015).

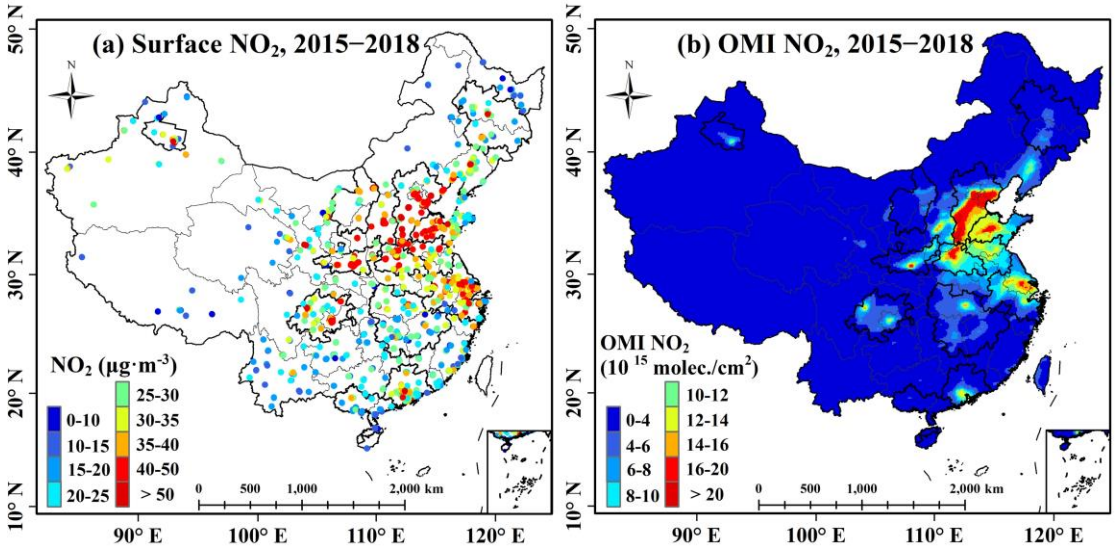

Figure 2. Spatial distributions of annual average (a) surface NO_2 concentrations and (b) tropospheric column NO_2 (XNO_2) in China from 2015−2018.

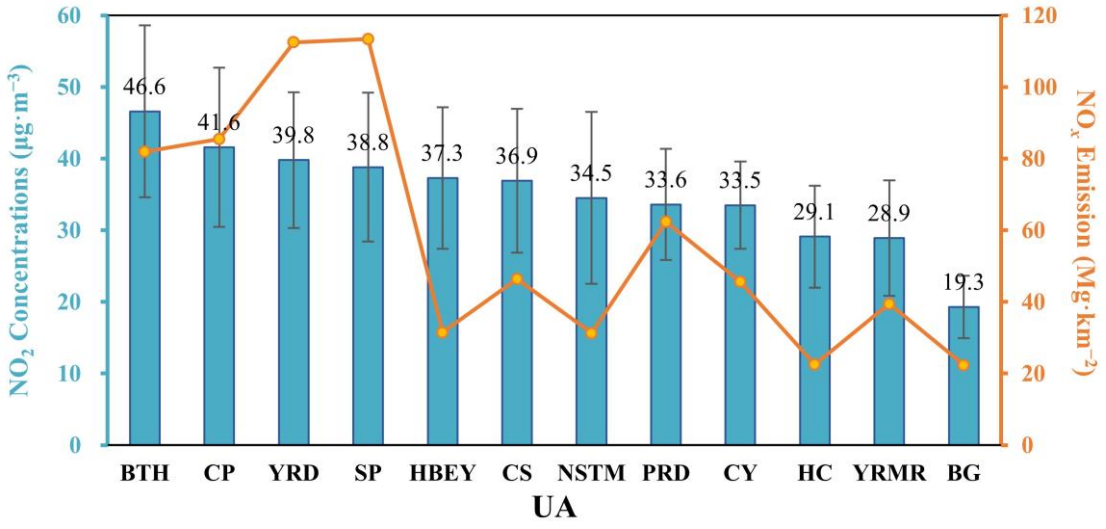

Figure 3. Annual mean NO_2 concentrations from 2015−2018 and annual NO_x

emissions in 2012 (Emission data are from MEIC 2012) in the 12 UAs.

3.1.2. Spatial autocorrelation of NO_2 concentrations

Air pollutants in adjacent areas generally interact through atmosphere transmission (Yan et al., 2018). Spatial autocorrelation analysis measures the interactions of air pollutants in adjacent areas. For example, based on emission inventory data, Fang (2015) used global and local spatial autocorrelation methods to analyze the spatial autocorrelation of urban air quality indexes and quantitatively evaluated the comprehensive effect of urbanization process on air quality in China. In this study, the local Moran's index (LMI) (Anselin, 1995) was used to identify the spatial autocorrelation distribution and the agglomeration pattern (AP) of atmospheric NO_2 pollution; the *Z*-score was used to test the significance of the spatial autocorrelation. Details for the calculations of LMI and the *Z*-score can be found in Li and Zhang (2011). A *Z*-score is greater than 1.96 (95% confidence interval) shows a significantly positive autocorrelation between a city and the surrounding ones. The city and its neighbors could both have relatively high or low concentrations; these possibilities are called high-high and low-low APs, respectively. A *Z*-score less than −1.96 shows a significantly negative autocorrelation and can also be divided into high-low and low-high APs based on different concentrations. A *Z*-score greater than −1.96 but less than 1.96 represents a city with no significant correlation with surrounding cities. The operation of the spatial autocorrelation calculation was implemented with the GeoDa (version 1.12.1.139) software (http://geodacenter.asu.edu/software/downloads).

Figure 4 shows the patterns of the spatial autocorrelations of averaged NO_2 concentrations in different prefecture-level cities in China. The distribution of NO_2 pollution is spatially autocorrelated with two high-high APs. The first is located in the North China Plain, the Guanzhong Plain, and most of Shanxi Province, which form the area with the worst air pollution in China. This AP covers four UAs and includes BTH, SP, CP, and CS. The area approximately overlaps with that covered by the BTH air

pollution transmission channel cities ("2 + 26" cities and Fenwei Plain cities) (Feng et al., 2019b; Cheng et al., 2019; Liu and Yuan, 2020), indicating a strong NO_2 pollution interaction in this area. The second high-high AP is located in YRD and includes southern Jiangsu and the adjacent cities in Jiangsu and Anhui provinces. Previous studies showed the strong interactions of air pollution in this area (He et al., 2017b; Bai et al., 2018). The low-low NO_2 APs are primarily distributed in the remote areas of China. Among the 12 UAs, only BG shows low-low AP because of the coastal geographical location and good air diffusion conditions. The number of cities showing high-high and low-low AP account for 18.9% and 17.7%, respectively. Compared to $PM_{2.5}$, the distributions of high-high NO_2 APs are more concentrated, because the high-high NO_2 APs are primarily located in BTH, SP, CS, CP, and YRD. The agglomeration characteristics of $PM_{2.5}$ are not only present in the aforementioned UAs, but also in HC, YRMR, NSTM, and CY (Shen et al., 2019).

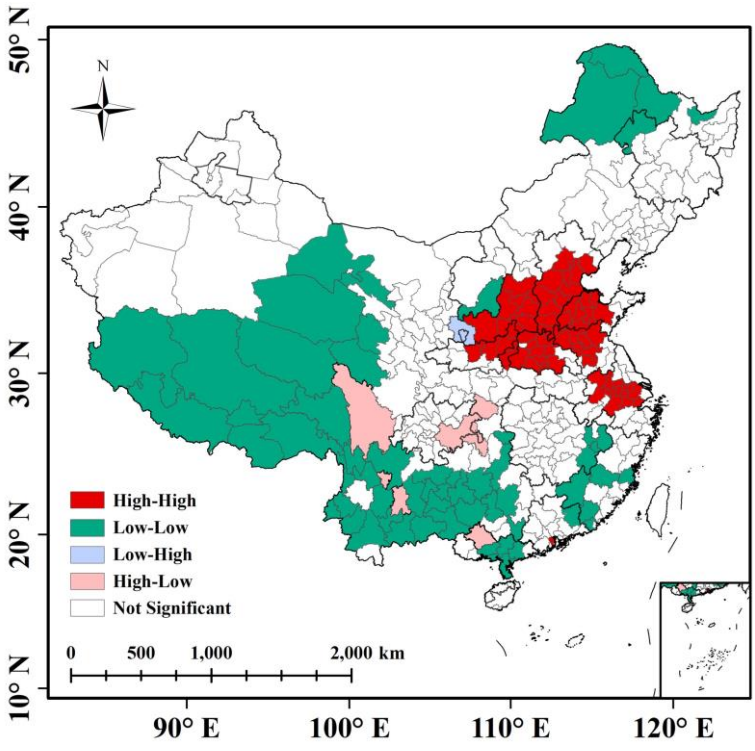

Figure 4. Spatial agglomeration of averaged NO_2 autocorrelations in China from 2015−2018.

3.2. Temporal variability of NO_2 concentrations

3.2.1. Monthly variations

Figure 5 shows the monthly mean surface NO_2 concentrations in the 12 UAs from June 2014 to May 2019. Clearly, typical UAs have remarkable monthly NO_2 variations. Monthly variations throughout the year for different UAs are similar with high values in January and December and low values in July or August, showing a typical "U" shape. Since the monthly variation of anthropogenic NO_x emissions in China usually presents a "W" shape (Qu et al., 2017), which is basically opposite to those of the atmospheric NO_2 concentrations, thus the monthly NO_2 variation is dominated by the changing of meteorological factors (Kui and Liu, 2019). Generally, in warm season, there are higher temperature and boundary layer height, stronger radiation, and more rainfall, resulting the lower NO_2 concentrations (Wei et al., 2012). Additionally, most UAs experience a small peak in March or April, i.e., the concentration of NO_2 decreases quickly from January to February, and then, it increases again, which is attributed to the Chinese Spring Festival, generally happening in February. From 2014 to 2019, the seasonal variations are different among different UAs. BTH and HBEY have much lower concentrations during the winter of 2017; YRMR, CY, PRD, and BG have relatively lower concentrations during the winters of 2015 and 2018. In BTH, YRD, CS, and CY, the NO_2 concentrations increase in 2017 and decrease in 2018; in HC, CP, SP, NSTM, and BG, the NO_2 concentrations show a slightly downward trend from 2014 to 2019—especially in HC; in PRD and HBEY, the NO_2 show an upward trend that is especially pronounced in HBEY.

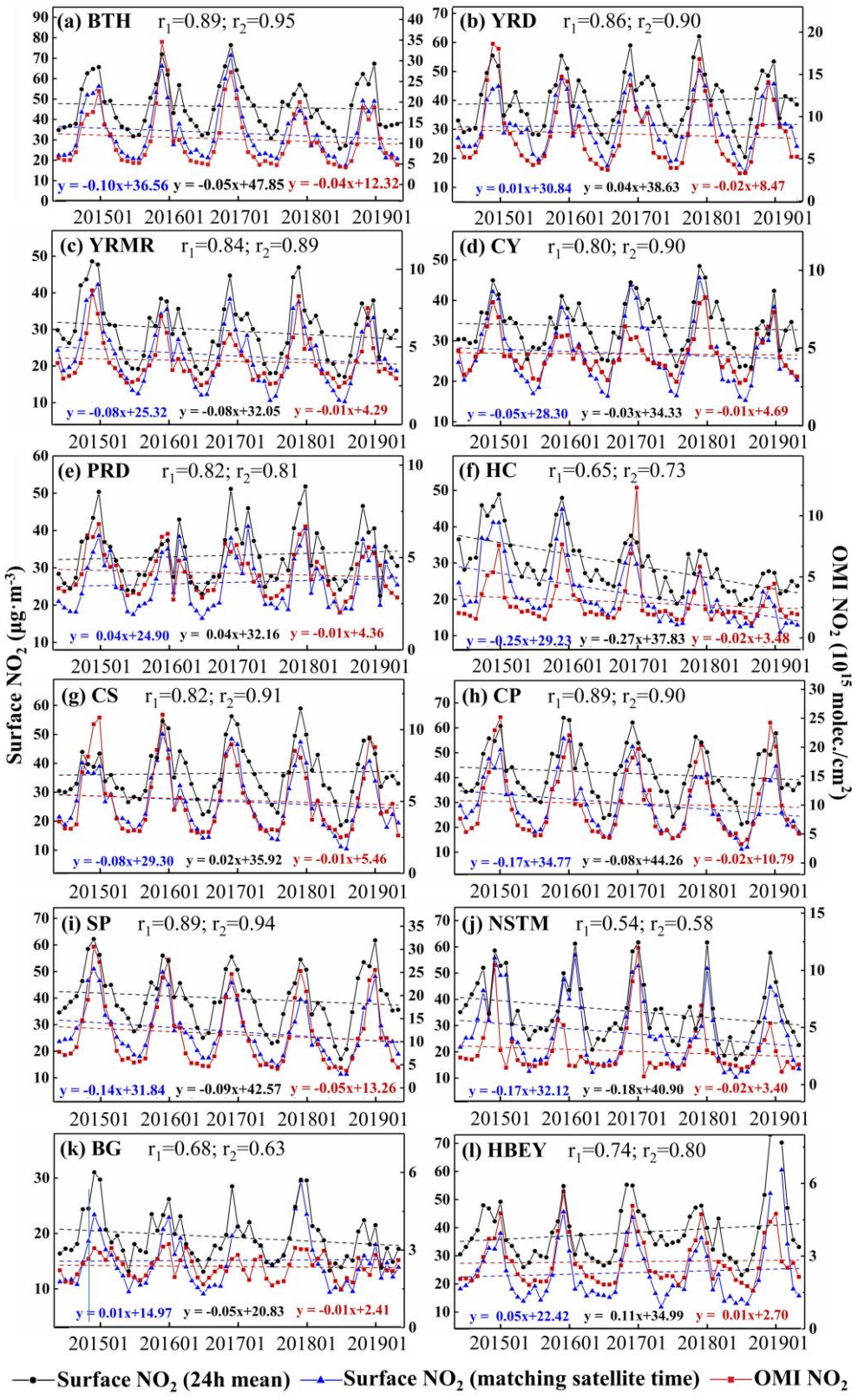

Figure 5. Time series of monthly surface NO_2 concentrations and OMI-retrieved tropospheric NO_2 columns in the 12 UAs; r_1 is the Pearson correlation coefficient between OMI-retrieved tropospheric NO_2 columns and the 24 h mean values of surface

328 NO_2 concentrations; r_2 is the Pearson correlation coefficient between OMI-retrieved
329 tropospheric NO_2 columns and the mean values of surface NO_2 concentrations from
330 12:00 to 17:00, coinciding with the local overpass time of the Aura satellite.

331 Figure 5 also shows the monthly mean OMI-retrieved XNO_2 concentrations. There
332 are interannual variation differences between surface and column concentrations. For
333 example, in BTH, the XNO_2 shows a peak in December 2015 before decreasing each
334 subsequent year, but the surface concentration is the highest in December 2016. In PRD,
335 the XNO_2 and surface NO_2 show slightly downward and upward trends, respectively.
336 In HBEY, there is no notable trend in the XNO_2 but a significantly upward trend in the
337 surface NO_2. In HC, the surface NO_2 decreases each year, but XNO_2 increases, peaks
338 in December 2016, and rapidly decreases. Xie et al. (2018) found large differences in
339 the interannual variations of the surface and column concentrations. One possible
340 reason for the discrepancy is that surface NO_2 was measured hourly, whereas XNO_2 is
341 sensed at most once a day (at the satellite transit time). Mean surface NO_2
342 concentrations near the satellite transit times are also shown in Figure 5. Here, the
343 observations during the afternoon (from 12:00 to 17:00) are used. The interannual
344 changes of surface NO_2 at the satellite transit times are relatively consistent with XNO_2
345 in most UAs. The Pearson linear correlation coefficients between the two data are
346 greater than 0.8, except for in HC, BG, and NSTM. A possible reason for the low
347 correlations in HC, BG, and NSTM is the shortage of valid retrievals in these three UAs
348 because of the extensive cloud cover or strong surface albedo (Boersma et al., 2018).
349 BG, located in southernmost mainland China, experiences abundant cloud coverage and
350 precipitation. PRD is located near BG and has a relatively low (0.81) correlation
351 coefficient. NSTM, in western China is surrounded by desert and HC, in northeast
352 China, has the longest snow cover of the 12 UAs. Desert or snow-covered areas
353 generally feature high surface albedo. These indicate that the satellite retrievals could
354 not well reflect the temporal variations in surface NO_2 concentration probably due to

that the changes of NO_2 concentrations during the daytime may be different from those during the nighttime. Besides, the monthly XNO_2 retrievals are less representative in those areas with heavy cloud cover and strong albedo.

3.2.2. Interannual variations

Figure 5 shows that the interannual variations of NO_2 in winter and summer are not consistent in most UAs. A possible reason is that pollution is much more severe and control measures much stricter during the winter; during the summer, pollution is much less intense, and control measures may be more lenient (SCPRC, 2018). To be clear, yearly NO_2 changes in winter and summer are shown in Figure 6. In addition, annual averaged NO_2 concentrations are given in Figure 6 to better represent the interannual trends. The trends in some UAs, such as CP, SP, NSTM, HC, and BG, are similar (Figure 5); therefore, this manuscript only presents the interannual variations and their causes in the five national UAs, HC, and HBEY.

The interannual variabilities of NO_2 concentrations in winter are more significant and different—except for HC—than that in summer. In BTH and YRD, the NO_2 concentrations changed little from 2014 to 2017 but significantly decreased in 2018 during the summer; in winter, however, they first increased, peaking in 2016 and 2017 in BTH and YRD, respectively, before decreasing. In YRMR, summer concentrations decreased significantly from 2014 and 2015 but showed little change from 2015 to 2018; winter concentrations decreased in 2015, increased from 2015 to 2017, and significantly decreased in 2018. CY and HBEY showed a gradual downward trend in summer concentrations with an increase in 2017; however, during the winter, the changes between CY and HBEY were significantly different. CY experienced changes similar to those of YRMR, whereas HBEY showed a significant increase. In PRD, there were no significant changes from 2014 to 2018 during the summer, and in winter, there was no significant trend as well, but featured large interannual variations. In HC, concentrations in summer and winter gradually decreased from 2014 to 2018, but the

decline rate was faster in winter. Additionally, the interannual variations of the annual mean concentrations in all UAs agreed with the changes in summer, indicating that—in addition to the pollution control in winter—the government needs to pay attention to the NO_x control in the summer.

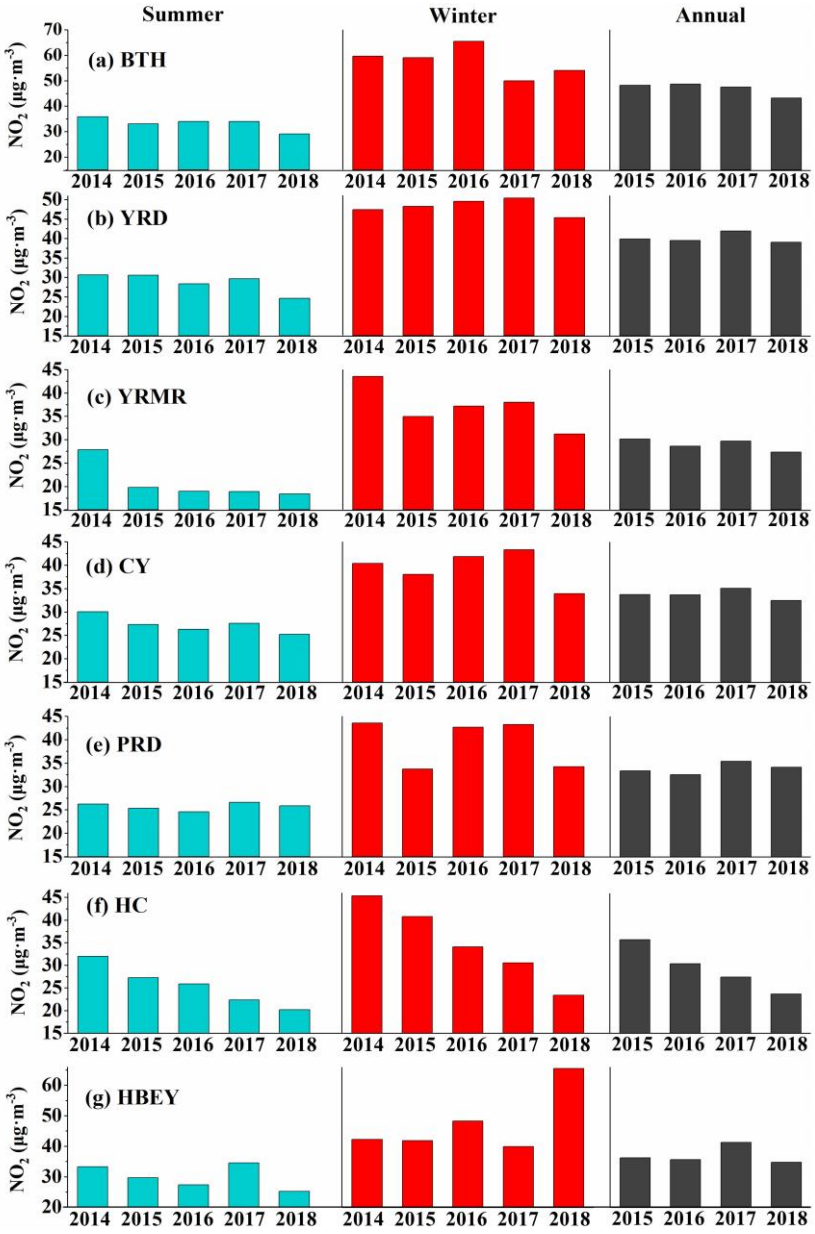

Figure 6. Interannual variations of summer, winter, and annual NO_2 concentrations in: (a) BTH, (b) YRD, (c) YRMR, (d) CY, (e) PRD, (f) HC, and (g) HBEY.

3.2.3. Frequency of daily mean concentrations

Figure 7 shows the frequency distributions of daily averaged NO_2 concentrations in the five national UAs, HC, and HBEY. We divided the concentrations into 8 sections and counted the frequency of each section in all seven UAs. The 8 concentration sections are 0−10 $\mu g \cdot m^{-3}$ (S1), 10−25 $\mu g \cdot m^{-3}$ (S2), 25−40 $\mu g \cdot m^{-3}$ (S3), 40−60 $\mu g \cdot m^{-3}$ (S4), 60−80 $\mu g \cdot m^{-3}$ (S5), 80−100 $\mu g \cdot m^{-3}$ (S6), 100−150 $\mu g \cdot m^{-3}$ (S7), and greater than 150 $\mu g \cdot m^{-3}$ (S8). The frequency generally shows a single-peak distribution, with the highest frequency appearing in S2 in all the UAs. As the concentration increased, the frequency rapidly decreased. In BTH, the frequency distribution of NO_2 was broader than in other UAs. In the range of greater than 80 $\mu g \cdot m^{-3}$ (Chinese Ambient Air Quality Standards (CAAQS) Grade II standard) (MEP, 2012), the frequency in BTH was significantly higher than that of other UAs, indicating severe NO_2 pollution in BTH.

The overall annual S2 frequency increased each year in the seven UAs, indicating a development towards low NO_2 concentration range and also affecting the frequency of other sections, whereas the interannual changes for sections greater than S2 varied by UA. In BTH, the S5 and S6 frequencies increased from 2015 to 2017 and decreased in 2018, but in the high sections (S7 and S8), the frequencies gradually decreased, indicating that extreme pollution was decreasing. In YRD, only S4 shows a gradually downward frequency, and an upward trend exists in the high sections. In YRMR, from S3 to S8, there was a downward trend for the frequency in each section, but in the sections greater than S5, there was an increase in 2017, coinciding with the relatively higher NO_2 concentration (Figure 6). In CY, the frequencies changed very little from 2015 to 2017 in each section, but decreased in most sections in 2018. In PRD, the overall frequencies changed slightly in each section, and in the high sections (greater than S5), the frequencies trended upward. In HBEY, there was no significant trend in S3, but all sections greater than S3 featured downward trends with an increase in 2017. In HC, the frequencies decreased each year in all sections greater than S2.

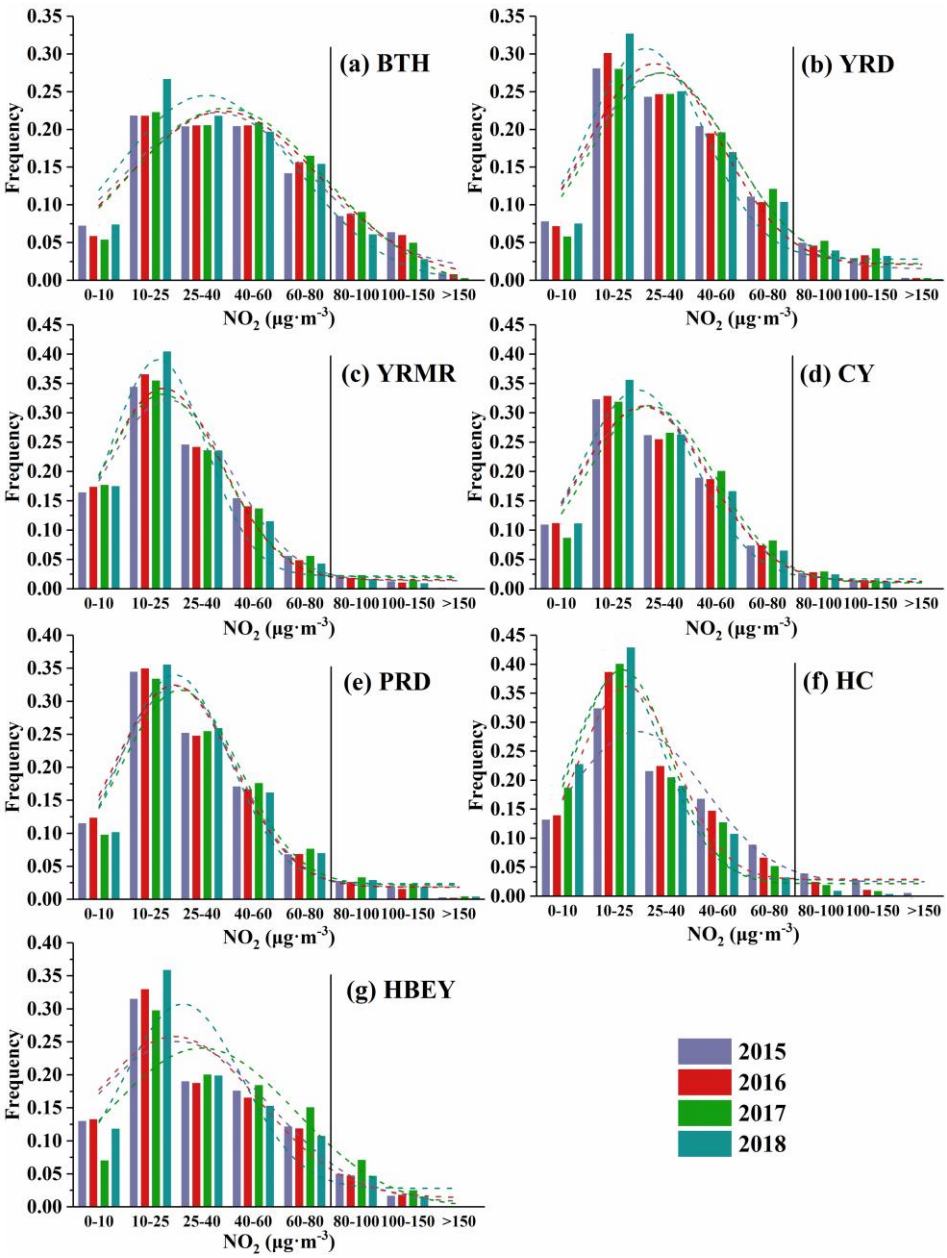

Figure 7. Interannual variations of the frequency distributions of the observed daily mean NO_2 concentrations for the five national UAs, HC, and HBEY from 2015−2018. Black lines represent the CAAQS Grade II standard (80 μg·m^{-3}) of NO_2. The dashed lines are Gaussian fitting curves.

3.3. Drivers of interannual variations

3.3.1. Model evaluation

The performance of the WRF model is critical to simulated the meteorologically

driven interannual NO_2 variations. Previous studies showed that temperature, relative humidity, and wind speed are the important meteorological factors in determining near-surface NO_2 variability (Harkey et al., 2015; Li et al., 2019). The simulated 2 m temperature (T2), 2 m relative humidity (RH2) and 10 m wind speeds (WS10) were evaluated against the ground-level observations. The observations from the meteorological measurement sites over China (Figure 1) were used for comparison. The data were obtained from the National Climate Data Center (NCDC) (ftp://ftp.ncdc.noaa.gov/pub/data/noaa/isd-lite/). Table 2 shows the evaluation results in each year. Overall, the WRF model well reproduced the domain-wide T2 and RH2 with fairly low deviations and high correlation coefficients. Their deviations are about -0.9 °C and 3.9, and correlation coefficients are greater than 0.93 and 0.85, respectively. The simulated WS10 was slightly overestimated due to the underestimation of the effects of urban topography and the lack of capture of all spatial features in the WRF model, which was also found in other studies using the WRF model (Jiang et al., 2012; Fan et al., 2015; Hu et al., 2016). PBLH is another meteorological factor that highly affect the diffusions of NO_2 and generally with large uncertainties in WRF simulations (Zhao et al., 2009), however, due to lack of PBLH observations, we did not evaluate the simulated PBLH in this study. According to criteria provided by Emery et al. (2001), the WRF model run in this study has acceptable performance in simulating meteorological parameters. In addition, it also could be found that the statistical results of each year are very close, indicating that the WRF simulations well reproduced the interannual variations of weather conditions.

We also evaluated the simulated NO_2 concentrations against the observations in each city in 2014 (Figure 8). The results show that the spatial variability of the simulated data is basically consistent with the observations, and their levels in most cities are close with each other. For temporal variations, the simulated and observed daily NO_2 concentrations also have good correlations, with correlation coefficients in range of 0.51 ~ 0.85 in different UAs. Overall, in both summer and winter seasons, the

simulated NO_2 concentrations are overestimated to a certain extent, the deviations are in the range of 10~30 $\mu g \cdot m^{-3}$ in most UAs. The deviations between the simulated and observed concentrations may be partly due to the use of emissions in 2012, since compared with 2012, the NO_x emission in 2014 was estimated to have declined by 13% (Zheng et al., 2018b). In addition, the large uncertainties in the emission inventory itself, the coarse model resolution (36 km) used in this study as well as the model structure also have contributions on the deviations (Kong et al., 2020).

Table 2. Evaluation for meteorological parameters simulated by the WRF model over 2014-2019

Meteorological parameters	Year	Sample Number	Mean Observation	Mean Simulation	MB	RMSE	NMB	NME	R
2m Temperature (°C)	2014	401	12.1	13.0	-0.9	2.9	-7.4	13.8	0.93
	2015	398	12.3	13.1	-0.8	2.7	-5.7	3.4	0.94
	2016	400	12.2	13.2	-1.0	3.0	-7.6	10.5	0.93
	2017	400	12.4	13.2	-0.8	2.6	-6.3	9.8	0.95
	2018	404	12.4	13.3	-0.9	3.3	-6.4	14.6	0.94
	2019	399	12.4	13.3	-0.9	2.8	-6.7	13.3	0.94
2 m Relative Humidity (%)	2014	401	63.8	59.7	4.1	9.4	6.7	11.8	0.85
	2015	398	64.9	61.9	3.0	9.7	5.3	3.7	0.86
	2016	400	65.8	61.7	4.1	8.8	6.7	8.7	0.87
	2017	400	64.0	60.1	3.9	9.8	6.9	9.7	0.85
	2018	404	64.1	60.2	3.9	11	7.4	12.3	0.86
	2019	399	63.6	59.7	3.9	9.2	6.6	11.5	0.85
10 m Wind Speed ($m \cdot s^{-1}$)	2014	401	3.0	2.6	0.4	1.0	18.0	28.9	0.60
	2015	398	3.1	2.6	0.5	1.0	19.6	11.8	0.65
	2016	400	3.1	2.7	0.4	1.0	17.5	19.2	0.64
	2017	400	3.1	2.6	0.5	1.0	17.5	19.3	0.66
	2018	404	3.1	2.7	0.4	1.1	18.3	30.6	0.64
	2019	399	3.0	2.6	0.4	1.0	16.3	28.6	0.63

Note: Sample Number is the number of sites with available observation for statistics. Units for Mean Observation, Mean Simulation, MB (Mean Bias), RMSE (Root Mean Squared Error) are given below the name of each parameter in the first column, and units for NMB (Normalized Mean Bias), and NME (Normalized Mean Error) are %.

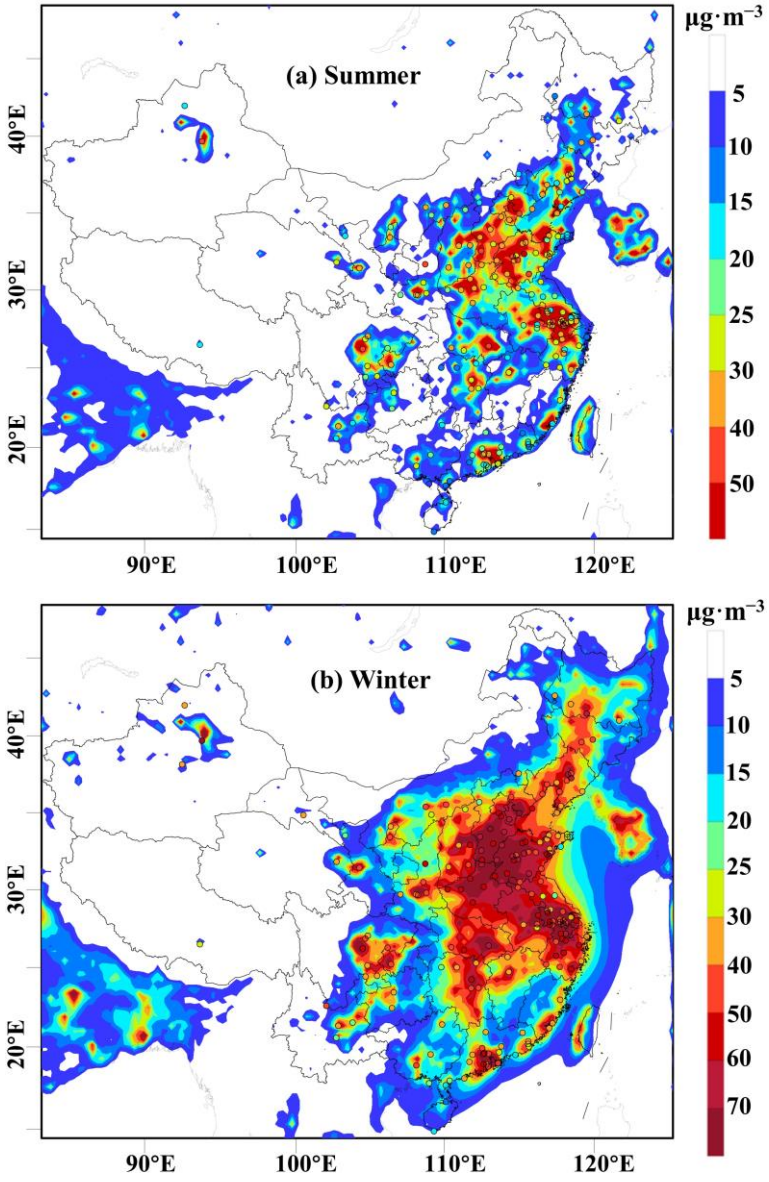

Figure 8. Comparisons of the averaged simulated (shaded) and observed (dotted) NO_2 concentrations in (a) summer and (b) winter of 2014.

3.3.2. The contributions of weather and emission changes on NO_2 concentrations

The variations of NO_2 concentrations are usually determined by three major factors: emissions, meteorology, and atmospheric chemical processes. Generally, the

interannual variation of NO_2 caused by atmospheric chemical processes is not independent, but closely related to the changes in meteorological conditions and emissions. Meteorological conditions directly affect the concentration of atmospheric oxidants, thereby indirectly affecting the consumption of NO_2 by these oxidants. Meanwhile, weather factors like temperature also directly affect the reaction rate of atmospheric oxidants with NO_2 (Jacob, 1999). In addition, the concentration of atmospheric oxidants is also closely related to the changes in anthropogenic emissions (Vermeuel et al., 2019). Take ozone as an example, which is one of the main atmospheric oxidants that oxidize NO_2, besides weather condition, its concentration is mainly dominated by the emissions of its precursors (i.e., NO_x and volatile organic compounds, Wang et al., 2019). Therefore, researchers usually only attribute the inter-annual variations in air pollutant concentrations to the changes in meteorological conditions and emissions. For example, Liu et al. (2017b) explores the major reasons behind the severe pollution in BTH from the perspective of meteorology and emissions, Xu et al. (2019b) and Xu et al. (2020) applied the WRF-CMAQ modeling system to investigate the impact of meteorological conditions and emission reduction on $PM_{2.5}$ pollution in China, and Zhang et al. (2019a) used WRF-CMAQ model to simulate variations in $PM_{2.5}$ concentrations from 2013 to 2017, and separate the contributions of $PM_{2.5}$ variations to anthropogenic emissions and meteorological factors.

The emission-fixed and meteorology-varied simulation could provide the contribution of meteorological conditions to variations. By comparing the observed and simulated NO_2 concentrations, emission-related NO_2 contributions could also be derived (observed minus simulated). As shown in section 3.3.1, there are unignorable deviations between the simulated and observed NO_2 concentrations. To avoid the impact of these deviations, when comparing the trends between the simulations and observations, for each UA, we used relative changes from 2014 levels for both simulated and observed NO_2; and when quantifying the weather and emission contributions, for each two consecutive years, we adjusted the simulated concentration

499 in the first year to be equal to the observed one, and scaled the simulated concentration
500 in the second year using the ratio of the simulated NO_2 to the observed one in the first
501 year (Zhang et al., 2019a).

502 Figure 9 shows the interannual variations of observed and simulated NO_2 trends
503 for the summer and winter in the five national UAs, HC, and HBEY from 2015–2018.
504 Simulated NO_2 generally shows a much weaker trend and smaller interannual variations
505 in each UA than the observed levels. In summer, the simulated NO_2 in BTH, YRD,
506 YRMR, CY, and HBEY is rather stable from 2014 to 2018, indicating that the decrease
507 of observed NO_2 in 2015 and 2018 in BTH and the downward trends from 2014–2016
508 and 2014–2018 in HBEY and CY respectively, are primarily attributed to emission
509 reductions. Zhang et al. (2019c) showed that in YRD, the decline of $PM_{2.5}$ was far
510 greater than the contribution of the improved meteorological conditions. Additionally,
511 the simulated NO_2 decrease in 2018 in YRD and HBEY, and in 2015 in YRMR, of a
512 much lower magnitudes than the observed reductions, suggesting that these decreases
513 are influenced by both weather changes and emission reductions. In PRD, the trend of
514 the simulated NO_2 is opposite to that of the observed, indicating that the interannual
515 variations are dominated by emission changes. During the wintertime, in YRD, YRMR,
516 CY, and PRD, the simulated NO_2 is very stable in the study period, implying that the
517 interannual changes of NO_2 concentrations in these UAs are primarily attributed to
518 emission changes. In BTH and HBEY, the changes of the simulated NO_2 are basically
519 in line with the ones of the observed NO_2. From 2014 to 2016, the observed changes in
520 BTH and HBEY are completely consistent with those of the simulations, indicating that
521 the changes are exclusively caused by the weather. However, from 2016 to 2018, the
522 simulated changes in BTH and HBEY are much weaker than the observed ones,
523 especially for the significant rise in 2018 in HBEY, suggesting the important
524 contribution of emission changes. In HC, the simulated NO_2 have downward trends in
525 both summer and winter, but are much weaker than the observed changes, indicating
526 that the gradual decrease in NO_2 concentrations in summer and winter are the result of

the combined effects of meteorological conditions and emission reductions. Therefore, the interannual variations of NO_2 are primarily dominated by the emissions changes. Nevertheless, the contributions from the meteorological changes are also important and can be dominant in some regions or seasons. This finding is consistent with the drivers of improved $PM_{2.5}$ concentrations in China from 2013 to 2017 that the anthropogenic emission is the dominant contribution, and the interannual meteorological variations could significantly alter $PM_{2.5}$ concentrations as well (Zhang et al., 2019a).

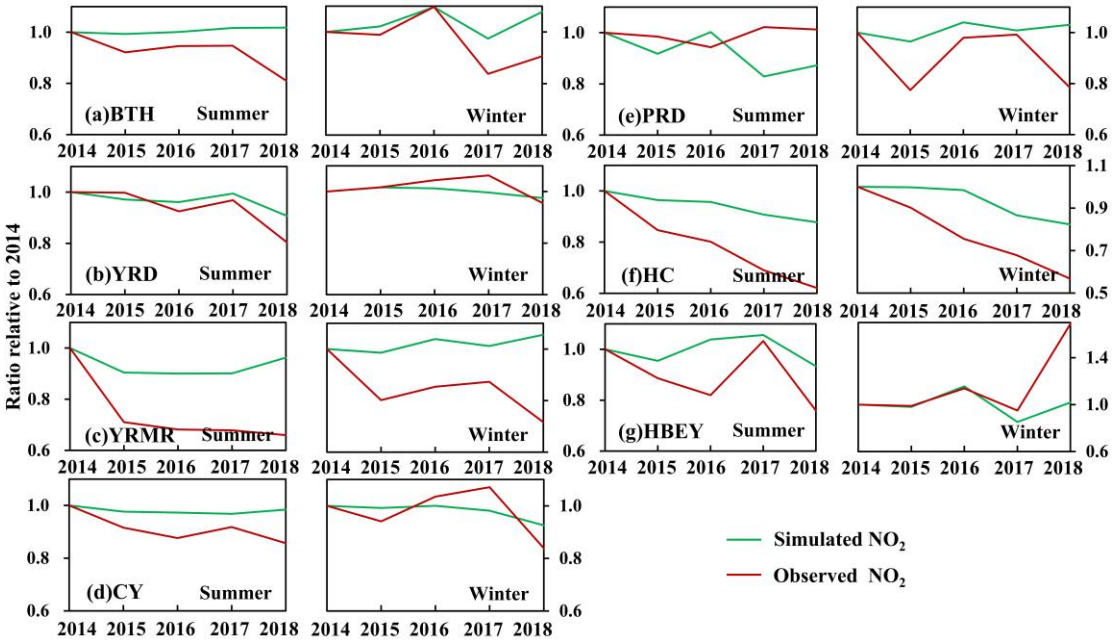

Figure 9. Comparisons of the simulated and observed trends for the mean NO_2 in summer and winter from 2014−2018 in the five national UAs, HC, and HBEY.

Figure 10 shows the quantitative contributions of the changes of meteorological conditions and anthropogenic emissions on the variations in NO_2 concentrations in the five national UAs, HC, and HBEY. In BTH, anthropogenic emission reductions in the summers of 2015 and 2018 reduced the NO_2 concentration by 2.8 and 5.0 $\mu g \cdot m^{-3}$, respectively, whereas the influence of meteorological conditions in winter was more pronounced than in other regions. We estimated that variation in meteorological conditions changed NO_2 concentrations in 2015, 2016, 2017, and 2018 by 1.3, 4.3, −7.3, and 5.3 $\mu g \cdot m^{-3}$, respectively. PBLH and wind speed changes are the primary

meteorological factors that affect NO_2 concentrations (Figure S3). Zhang et al. (2019c) reported that during the winter of 2017, meteorological drivers played a very significant role in reducing $PM_{2.5}$ in BTH. In the winter of 2018 in YRD and CY, emission reductions contributed 78.5% and 73.8% of the NO_2 concentration reductions, respectively. Similarly, Zhang and Geng (2019) found that, although the interannual variations in meteorological conditions can partially explain the reduction in $PM_{2.5}$ pollution, the decrease of $PM_{2.5}$ pollution in the winter of 2018 in YRD was dominated by emissions reduction. Anthropogenic emission reductions accounted for 66.9% of the 5.4 $\mu g \cdot m^{-3}$ decrease in NO_2 in YRMR during the summer of 2015. Additionally, in the winters of 2015 and 2018 in YRMR, and in the winter of 2015 and 2018 in PRD, the emissions reduction contributed to decreases of NO_2 concentrations by 8.0, 8.5, 8.3, and 10.0 $\mu g \cdot m^{-3}$, respectively. However, emission control in PRD failed in some years, and anthropogenic emissions caused an increase in NO_2 concentration. For example, anthropogenic emissions in PRD in the summer of 2017 and in the winter of 2016 caused NO_2 to rise by 6.3 $\mu g \cdot m^{-3}$. Due to the significant increase in wind speed (Figure S3), the meteorological conditions of PRD in the summer of 2017 reduced NO_2, but were outweighed by the impact of interannual changes in emissions that caused an overall rise in NO_2 concentration. In HC, the contribution of emissions reduction is much more significant than that of meteorological conditions. In HBEY, the impact of anthropogenic emissions during the summer caused NO_2 changes of −4.8 $\mu g \cdot m^{-3}$, 6.6 $\mu g \cdot m^{-3}$, and −5.1 $\mu g \cdot m^{-3}$ in 2016, 2017, and 2018, respectively. Of the large NO_2 increase of 31.4 $\mu g \cdot m^{-3}$ in the winter of 2018 in HBEY, 23.5 $\mu g \cdot m^{-3}$ was caused by changes in anthropogenic emissions, while the remaining 7.9 $\mu g \cdot m^{-3}$ is attributed to the weather changes. Overall, from 2014 to 2018, except for the summer of PRD and the winter of HBEY, the NO_2 concentrations in other regions and seasons decreased significantly, and these decreases are mainly attributed to the emission changes, which is consistent with the NO_x emission declines in inventory since 2013 (Zheng et al., 2018b). The slight increase in PRD may be related to the fact that the NO_x emission in

PRD mainly comes from motor vehicles (Zhong et al., 2018), while the declines of NO_x emission in recent years in China is mainly attributed to the emission reductions in power plants (Zheng et al., 2018a; Zheng et al., 2018b). The significant increase of NO_2 in HBEY from 2017 to 2018 may be related to the coal-to-gas policy implemented began in the autumn and winter of 2018 (Zhao et al., 2020), since HBEY is an important base for converting coal to natural gas in China.

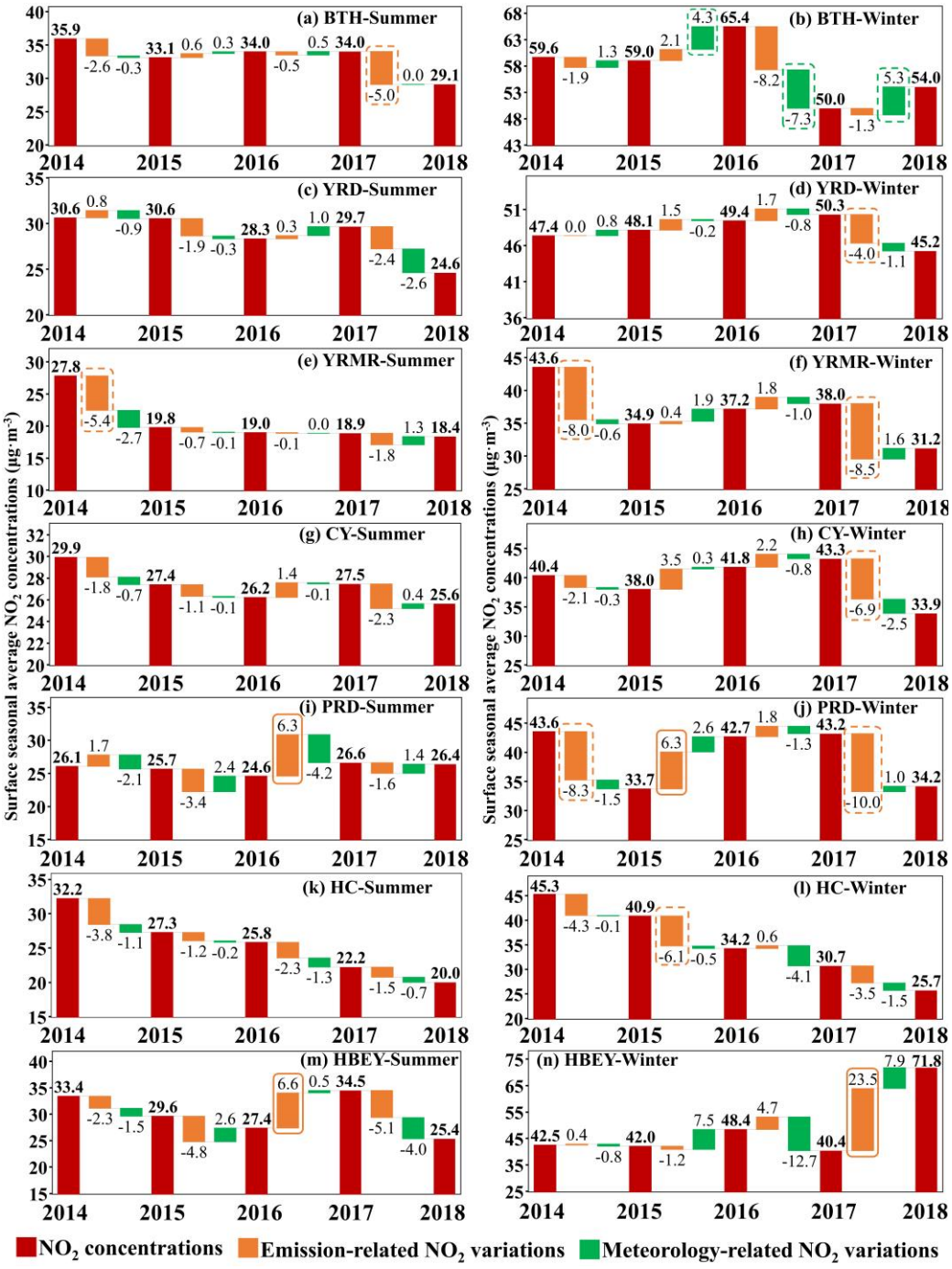

Figure 10. The yearly changes in NO_2 concentrations contributed by anthropogenic

emission and meteorological condition changes between 2014 and 2018 for the five national UAs, HC, and HBEY. The dotted green boxes indicate a predominantly meteorological influence. The dotted orange boxes indicate a significant reduction of NO_2 from anthropogenic emissions control. The solid orange boxes indicate a large NO_2 increase caused by anthropogenic emissions.

4. Summary and Conclusions

In this study based on hourly NO_2 observations in China from June 2014 to May 2019, we analyzed the spatial distribution of NO_2 concentrations and the temporal variations in 12 typical UAs. We found that BTH, YRD, and CP had the highest NO_2 concentrations, followed by SP, CS, and HBEY; HC, YRMR, and BG had the lowest concentrations—even lower than the national average. The OMI XNO_2 retrievals showed a spatial distribution similar to that of ground observations. These spatial distributions were dominated by the emission strength of NO_x and are also highly affected by weather conditions. The interannual variations of NO_2 decreased in 2016 in BTH and in 2017 in YRD, CS, and CY; HC, CP, SP, NSTM, and BG featured a downward trend from 2014 to 2019, especially in HC, while in PRD and HBEY, it shows an upward trend, especially pronounced in HBEY.

We quantitatively study the drivers of NO_2 interannual variations using the WRF−CMAQ model with fixed anthropogenic emissions and variational meteorological conditions and find that the interannual variations of NO_2 are primarily dominated by emissions changes, while the contribution from meteorological changes cannot be ignored as well. In BTH, for example, meteorological conditions caused NO_2 changes of more than 5 $\mu g \cdot m^{-3}$ in the winters of 2017 and 2018. In the winter of 2018 in YRD and CY, emission reductions contributed 78.5% and 73.8% of the NO_2 reductions, which is same for $PM_{2.5}$ that the improvement of $PM_{2.5}$ pollution was dominated by emission reductions. In the winters of 2015 and 2018, the emissions reduction contributed to significant NO_2 decreases of 8.0 and 8.5 $\mu g \cdot m^{-3}$ in YRMR and

of 8.3 and 10.0 μg·m^{-3} in PRD. However, in PRD, emissions increase NO_2 to more than 6 μg·m^{-3} in the summer of 2017 and the winter of 2016. In the two regional UAs, the contribution of emission reductions is much more significant than that of meteorological conditions, especially in HBEY, the impact of anthropogenic emissions caused a change of 6.6 μg·m^{-3} in the summer of 2017 and a huge increase of 31.4 μg·m^{-3} in the winter of 2018.

Because the simulation error of the WRF−CMAQ model will be transmitted downward, the "relative change" method (the change in the next year is relative to that of the previous year) was used to partially reduce the impact of model simulation uncertainty (Xu et al., 2019b). Because comprehensive studies of NO_2 characteristics and a quantitative analysis of the effects related to meteorology and emissions on NO_2 concentrations in several UAs across the country is rare, this study may provide a basic understanding of current NO_2 pollution and provide a scientific basis for policy-makers to propose effective strategies.

Declaration of competing interest

The authors declare that they have no known competing financial interests or personal relationships that could have appeared to influence the work reported in this paper.

Acknowledgement

This work is supported by the National Key R&D Program of China (Grant No: 2016YFA0600204) and the National Natural Science Foundation of China (Grant No: 41571452). We are grateful to the High Performance Computing Center (HPCC) of Nanjing University for doing the numerical calculations in this paper on its blade cluster system.

Appendix A. Supplementary data

Supplementary data to this article can be found online.

References

Ai, J., Sun, Y., Zheng, F., Ni, C., Gui, K., Zhang, X., Jiang, W., Liao, T., 2018. The spatial temporal variation and factor analysis of the tropospheric NO_2 columns in the Sichuan Basin from 2005 to 2016. Atmospheric Pollution Research. 9, 1157-1166. https://doi.org/10.1016/j.apr.2018.04.001.

Anand, J.S., Monks, P.S., 2017. Estimating daily surface NO_2 concentrations from satellite data – a case study over Hong Kong using land use regression models. Atmospheric Chemistry and Physics. 17, 8211-8230. https://doi.org/10.5194/acp-17-8211-2017.

Anselin, L., 1995. Local indicators of spatial association—LISA. Geographical Analysis. 27, 93-115. https://doi.org/10.1111/j.1538-4632.1995.tb00338.x

Bai, L., Jiang, L., Zhou, H., Chen, Z., 2018. Spatio-temporal characteristics of air quality index and its driving factors in the Yangtze River Economic Belt: An empirical study based on bayesian spatial econometric model. Scientia Geographica Sinica. 38, 2100-2108. (in Chinese).

Bauwens, M., Compernolle, S., Stavrakou, T., Muller, J.F., van Gent, J., Eskes, H., Levelt, P.F., van der, A.R., Veefkind, J.P., Vlietinck, J., Yu, H., Zehner, C., 2020. Impact of coronavirus outbreak on NO_2 pollution assessed using TROPOMI and OMI observations. Geophys Res Lett. 10.1029/2020GL087978, e2020GL087978. https://doi.org/10.1029/2020GL087978.

Binkowski, F., Roselle, S.J., 2003. Models-3 Community Multiscale Air Quality (CMAQ) model aerosol component 1. Model description. J. Geophys. Res. 108. https://doi.org/10.1029/2001JD001409.

Boersma, K. F., Eskes, H., Richter, A., De Smedt, I., Lorente, A., Beirle, S., Van Geffen,

J., Peters, E., Van Roozendael, M. and Wagner, T., 2017. QA4ECV NO_2 tropospheric and stratospheric vertical column data from OMI (Version 1.1) [Data set]. Royal Netherlands Meteorological Institute (KNMI). http://doi.org/10.21944/qa4ecv-no2-omi-v1.1.

Boersma, K.F., Eskes, H.J., Richter, A., De Smedt, I., Lorente, A., Beirle, S., van Geffen, J.H.G.M., Zara, M., Peters, E., Van Roozendael, M., Wagner, T., Maasakkers, J.D., van der A, R.J., Nightingale, J., De Rudder, A., Irie, H., Pinardi, G., Lambert, J.-C., Compernolle, S.C., 2018. Improving algorithms and uncertainty estimates for satellite NO_2 retrievals: results from the quality assurance for the essential climate variables (QA4ECV) project. Atmospheric Measurement Techniques. 11, 6651-6678. https://doi.org/10.5194/amt-11-6651-2018.

Bucsela, E.J., Krotkov, N.A., Celarier, E.A., Lamsal, L.N., Swartz, W.H., Bhartia, P.K., Boersma, K.F., Veefkind, J.P., Gleason, J.F., Pickering, K.E., 2013. A new stratospheric and tropospheric NO_2 retrieval algorithm for nadir-viewing satellite instruments: Applications to OMI. Atmospheric Measurement Techniques Discussions. 6, 1361-1407. https://doi.org/10.5194/amtd-6-1361-2013.

Carmona-Cabezas, R., Gomez-Gomez, J., Gutierrez de Rave, E., Jimenez-Hornero, F.J., 2020. Checking complex networks indicators in search of singular episodes of the photochemical smog. Chemosphere. 241, 125085. https://doi.org/10.1016/j.chemosphere.2019.125085.

Castellanos, P., Boersma, K.F., 2012. Reductions in nitrogen oxides over Europe driven by environmental policy and economic recession. Sci Rep. 2, 265. https://doi.org/10.1038/srep00265.

Chai, F., Gao, J., Chen, Z., Wang, S., Zhang, Y., Zhang, J., Zhang, H., Yun, Y., Ren, C., 2014. Spatial and temporal variation of particulate matter and gaseous pollutants in 26 cities in China. Journal of Environmental Sciences. 26, 75-82. https://doi.org/10.1016/s1001-0742(13)60383-6.

Chen, J., Zeng, J., Shi, C., Liu, R., Lu, R., Mao, S., Zhang, L., 2019a. Associations

between short-term exposure to gaseous pollutants and pulmonary heart disease-related mortality among elderly people in Chengdu, China. Environ Health. 18. https://doi.org/10.1186/s12940-019-0500-8.

Chen, W., Liu, Y., Wu, X., Bao, Q., Gao, Z., Zhang, X., 2019b. Spatial and temporal characteristics of air quality and cause analysis of heavy pollution in Northeast China. Environmental Science. 40, 4810-4823. https://doi.org/10.13227/j.hjkx.201807159. (in Chinese).

Chen, W., Tang, H., Zhao, H., 2015. Diurnal, weekly and monthly spatial variations of air pollutants and air quality of Beijing. Atmos Environ. 119, 21-34. https://doi.org/10.1016/j.atmosenv.2015.08.040.

Chen, Z., Chen, D., Zhao, C., Kwan, M.P., Cai, J., Zhuang, Y., Zhao, B., Wang, X., Chen, B., Yang, J., Li, R., He, B., Gao, B., Wang, K., Xu, B., 2020. Influence of meteorological conditions on $PM_{2.5}$ concentrations across China: A review of methodology and mechanism. Environ. Int. 139, 105558. https://doi.org/10.1016/j.envint.2020.105558.

Cheng, Y., Tingting, L., Yunlu, Z., Yaping, W., 2019. Spatiotemporal evolution and socioeconomic driving mechanism of air quality in Beijing-Tianjin-Hebei and surrounding areas ("2+26" Cities). Economic Geography. 39, 183-192. https://doi.org/10.15957/j.cnki.jjdl.2019.10.023. (in Chinese).

Duan, Y., Tian, G., Wu, B., Ma, G., Liu, Z., Lei, Y., 2017. Effect of urbanization on the spatio-temporal distribution of aerosols in Zhongyuan Metropolitan Area. Ecology and Environmental Sciences. 26, 1924-1934. https://doi.org/10.16258/j.cnki.1674-5906.2017.11.013. (in Chinese).

Emery, C., Tai, E., Yarwood, G., 2001. Enhanced meteorological modeling and performance evaluation for two Texas ozone episodes. in Final Report (ENVIRON International Corporation).

Fan, H., Zhao, C., Yang, Y., 2020a. A comprehensive analysis of the spatio-temporal variation of urban air pollution in China during 2014–2018. Atmospheric

Environment. 220, 117066. https://doi.org/10.1016/j.atmosenv.2019.117066.

Fan, Q., Lan, J., Liu, Y., Wang, X., Chan, P., Hong, Y., Feng, Y., Liu, Y., Zeng, Y., Liang, G., 2015. Process analysis of regional aerosol pollution during spring in the Pearl River Delta region, China. Atmospheric Environment. 122, 829-838.https://doi.org/10.1016/j.atmosenv.2015.09.013.

Fan, S.J., Heinrich, J., Bloom, M.S., Zhao, T.Y., Shi, T.X., Feng, W.R., Sun, Y., Shen, J.C., Yang, Z.C., Yang, B.Y., Dong, G.H., 2020b. Ambient air pollution and depression: A systematic review with meta-analysis up to 2019. Sci. Total. Environ. 701, 134721. https://doi.org/10.1016/j.scitotenv.2019.134721.

Fang, C., 2015. Progress and the future direction of research into urban agglomeration in China. Journal of Geographical Sciences. 25, 1003-1024. https://doi.org/10.1007/s11442-015-1216-5.

Fang, C.L., Wang, Z.B., Ma, H.T., 2018. The theoretical cognition of the development law of China's urban agglomeration and academic contribution. Acta Geographica Sinica. 73, 651-665. https://doi.org/10.11821/dlxb201804005. (in Chinese).

Feng, J., Zhang, Y., Li, S., Mao, J., Patton, A.P., Zhou, Y., Ma, W., Liu, C., Kan, H., Huang, C., An, J., Li, L., Shen, Y., Fu, Q., Wang, X., Liu, J., Wang, S., Ding, D., Cheng, J., Ge, W., Zhu, H., Walker, K., 2019a. The influence of spatiality on shipping emissions, air quality and potential human exposure in the Yangtze River Delta/Shanghai, China. Atmospheric Chemistry and Physics. 19, 6167-6183. https://doi.org/10.5194/acp-19-6167-2019.

Feng, S., Jiang, F., Jiang, Z., Wang, H., Cai, Z., Zhang, L., 2018. Impact of 3DVAR assimilation of surface $PM_{2.5}$ observations on $PM_{2.5}$ forecasts over China during wintertime. Atmos Environ. 187, 34-49. https://doi.org/10.1016/j.atmosenv.2018.05.049.

Feng, Y., Ning, M., Lei, Y., Sun, Y., Liu, W., Wang, J., 2019b. Defending blue sky in China: Effectiveness of the "Air Pollution Prevention and Control Action Plan" on air quality improvements from 2013 to 2017. J. Environ. Manage. 252, 109603.

https://doi.org/10.1016/j.jenvman.2019.109603.

Guenther, A.B., Jiang, X., Heald, Colette L., Sakulyanontvittaya, T., Duhl, T., 2012. The Model of Emissions of Gases and Aerosols from Nature version 2.1 (MEGAN2.1): an extended and updated framework for modeling biogenic emissions. Geoscientific Model Development. 5, 1471-1492. https://doi.org/10.5194/gmd-5-1471-2012.

Harkey, M., Holloway, T., Oberman, J., Scotty, E., 2015. An evaluation of CMAQ NO_2 using observed chemistry-meteorology correlations. Journal of Geophysical Research: Atmospheres. 120, 11,775-711,797. https://doi.org/10.1002/2015jd023316.

He, J., Gong, S., Yu, Y., Yu, L., Wu, L., Mao, H., Song, C., Zhao, S., Liu, H., Li, X., Li, R., 2017a. Air pollution characteristics and their relation to meteorological conditions during 2014–2015 in major Chinese cities. Environ Pollut. 223, 484-496. https://doi.org/10.1016/j.envpol.2017.01.050.

He, R., Zhu, L., Zhou, K., 2017b. Spatial autocorrelation analysis of air quality index (AQI) in eastern China based on residuals of time series models. Acta Sci. Circumstantiae. 37, 2459-2467. https://doi.org/10.13671/j.hjkxxb.2017.0049. (in Chinese).

Hu, J., Chen, J., Ying, Q., Zhang, H., 2016. One-year simulation of ozone and particulate matter in China using WRF/CMAQ modeling system. Atmospheric Chemistry and Physics. 16, 10333-10350. https://doi.org/10.5194/acp-16-10333-2016.

Hu, Q., Li, Y., 2016. Comparative research on air pollution statistical laws in Yunnan central, Guizhou central and Beibu Gulf urban agglomeration based on AQI. Ecological Economy. 32, 170-174+185. (in Chinese).

Hunova, I., Baumelt, V., Modlik, M., 2020. Long-term trends in nitrogen oxides at different types of monitoring stations in the Czech Republic. Sci. Total. Environ. 699, 134378. https://doi.org/10.1016/j.scitotenv.2019.134378.

Ielpo, P., Mangia, C., Marra, G.P., Comite, V., Rizza, U., Uricchio, V.F., Fermo, P., 2019. Outdoor spatial distribution and indoor levels of NO_2 and SO_2 in a high environmental risk site of the South Italy. Sci. Total. Environ. 648, 787-797. https://doi.org/10.1016/j.scitotenv.2018.08.159.

Jacob, D.J., 1999. Introduction to Atmospheric Chemistry. Princeton University, Princeton.

Jiang, F., Liu, Q., Huang, X., Wang, T., Zhuang, B., Xie, M., 2012. Regional modeling of secondary organic aerosol over China using WRF/Chem. Journal of Aerosol Science. 43, 57-73. https://doi.org/10.1016/j.jaerosci.2011.09.003.

Jiang, Y., Niu, Y., Xia, Y., Liu, C., Lin, Z., Wang, W., Ge, Y., Lei, X., Wang, C., Cai, J., Chen, R., Kan, H., 2019. Effects of personal nitrogen dioxide exposure on airway inflammation and lung function. Environ Res. 177, 108620. https://doi.org/10.1016/j.envres.2019.108620.

Jin, L., Berman, J.D., Zhang, Y., Thurston, G., Zhang, Y., Bell, M.L., 2019. Land use regression study in Lanzhou, China: A pilot sampling and spatial characteristics of pilot sampling sites. Atmos Environ. 210, 253-262. https://doi.org/10.1016/j.atmosenv.2019.02.043.

Just, A.C., Wright, R.O., Schwartz, J., Coull, B.A., Baccarelli, A.A., Tellez-Rojo, M.M., Moody, E., Wang, Y., Lyapustin, A., Kloog, I., 2015. Using high-resolution satellite aerosol optical depth to estimate daily $PM_{2.5}$ geographical distribution in Mexico City. Environ. Sci. Technol. 49, 8576-8584. https://doi.org/10.1021/acs.est.5b00859.

Kasparoglu, S., Incecik, S., Topcu, S., 2018. Spatial and temporal variation of O_3, NO and NO_2 concentrations at rural and urban sites in Marmara Region of Turkey. Atmospheric Pollution Research. 9, 1009-1020. https://doi.org/10.1016/j.apr.2018.03.005.

Kong, L., Tang, X., Zhu, J., Wang, Z., Fu, J.S., Wang, X., Itahashi, S., Yamaji, K., Nagashima, T., Lee, H.-J., Kim, C.-H., Lin, C.-Y., Chen, L., Zhang, M., Tao, Z.,

Li, J., Kajino, M., Liao, H., Wang, Z., Sudo, K., Wang, Y., Pan, Y., Tang, G., Li, M., Wu, Q., Ge, B., Carmichael, G.R., 2020. Evaluation and uncertainty investigation of the NO_2, CO and NH_3 modeling over China under the framework of MICS-Asia III. Atmospheric Chemistry and Physics. 20, 181-202. https://doi.org/10.5194/acp-20-181-2020.

Kui, B., Liu, X., 2019. Interregional differences, influencing factors and governance policy choices of air pollution—Based on the comparative analysis among Beijing-Tianjin-Hebei Region,Yangtze River Delta and Pearl River Delta. Bulletin of Science and Technology. 35, 197-202. https://doi.org/10.13774/j.cnki.kjtb.2019.08.036 (in Chinese).

Lamsal, L.N., Martin, R.V., Parrish, D.D., Krotkov, N.A., 2013. Scaling relationship for NO_2 pollution and urban population size: a satellite perspective. Environ. Sci. Technol. 47, 7855-7861. https://doi.org/10.1021/es400744g.

Levelt, P.F., van den Oord, G.H.J., Dobber, M.R., Malkki, A., Huib, V., Johan de, V., Stammes, P., Lundell, J.O.V., Saari, H., 2006. The ozone monitoring instrument. IEEE Transactions on Geoscience and Remote Sensing. 44, 1093-1101. https://doi.org/10.1109/tgrs.2006.872333.

Li, c., Zhang, z., 2011. Spatial statistics analysis of regional environmental pollution in China. Energy Procedia. 5, 163-168. https://doi.org/10.1016/j.egypro.2011.03.029.

Li, J., Yuan, F., Zhao, Y., Liu, L., 2020b. Effect of rainstorms on vegetation activities in eastern coastal area of China. Scientia Geographica Sinica. 40, 324-334. https://doi.org/10.13249/j.cnki.sgs.2020.02.018. (in Chinese).

Li, M., Zhang, Q., Kurokawa, J.-i., Woo, J.-H., He, K., Lu, Z., Ohara, T., Song, Y., Streets, D.G., Carmichael, G.R., Cheng, Y., Hong, C., Huo, H., Jiang, X., Kang, S., Liu, F., Su, H., Zheng, B., 2017b. MIX: a mosaic Asian anthropogenic emission inventory under the international collaboration framework of the MICS-Asia and HTAP. Atmospheric Chemistry and Physics. 17, 935-963. https://doi.org/10.5194/acp-17-935-2017.

826 Li, R., Cui, L., Li, J., Zhao, A., Fu, H., Wu, Y., Zhang, L., Kong, L., Chen, J., 2017a.
827 Spatial and temporal variation of particulate matter and gaseous pollutants in
828 China during 2014–2016. Atmos Environ. 161, 235-246.
829 https://doi.org/10.1016/j.atmosenv.2017.05.008.
830 Li, R., Wang, Z., Cui, L., Fu, H., Zhang, L., Kong, L., Chen, W., Chen, J., 2019. Air
831 pollution characteristics in China during 2015–2016: Spatiotemporal variations
832 and key meteorological factors. Science of The Total Environment. 648, 902-915.
833 https://doi.org/10.1016/j.scitotenv.2018.08.181.
834 Li, Y., Liu, J., Shi, G., Huangfu, Y., Zhang, X., Yang, Y., Feng, Y., 2020a. $PM_{2.5}$
835 pollution characteristics of winter and summer in Hohhot-Baotou-Ordos region,
836 China. Environmental Science. 41, 31-38.
837 https://doi.org/10.13227/j.hjkx.201904207. (in Chinese)
838 Li, Z., Lau, W.K.M., Ramanathan, V., Wu, G., Ding, Y., Manoj, M.G., Liu, J., Qian, Y.,
839 Li, J., Zhou, T., Fan, J., Rosenfeld, D., Ming, Y., Wang, Y., Huang, J., Wang, B.,
840 Xu, X., Lee, S.S., Cribb, M., Zhang, F., Yang, X., Zhao, C., Takemura, T., Wang,
841 K., Xia, X., Yin, Y., Zhang, H., Guo, J., Zhai, P.M., Sugimoto, N., Babu, S.S.,
842 Brasseur, G.P., 2016. Aerosol and monsoon climate interactions over Asia. Rev
843 Geophys. 54, 866-929. https://doi.org/10.1002/2015rg000500.
844 Lin, N., Wang, Y., Zhang, Y., Yang, K., 2019. A large decline of tropospheric NO_2 in
845 China observed from space by SNPP OMPS. Sci Total Environ. 675, 337-342.
846 https://doi.org/10.1016/j.scitotenv.2019.04.090.
847 Liu, C., Henderson, B.H., Wang, D., Yang, X., Peng, Z.R., 2016. A land use regression
848 application into assessing spatial variation of intra-urban fine particulate matter
849 ($PM_{2.5}$) and nitrogen dioxide (NO_2) concentrations in City of Shanghai, China. Sci.
850 Total. Environ. 565, 607-615. https://doi.org/10.1016/j.scitotenv.2016.03.189.
851 Liu, F., Beirle, S., Zhang, Q., van der, A.R., Zheng, B., Tong, D., He, K., 2017a. NO_x
852 emission trends over Chinese cities estimated from OMI observations during 2005
853 to 2015. Atmos Chem Phys. 17, 9261-9275. https://doi.org/10.5194/acp-17-9261-

2017.

Liu, M., Lin, J., Wang, Y., Sun, Y., Zheng, B., Shao, J., Chen, L., Zheng, Y., Chen, J., Fu, T.-M., Yan, Y., Zhang, Q., Wu, Z., 2018. Spatiotemporal variability of NO_2 and $PM_{2.5}$ over Eastern China: observational and model analyses with a novel statistical method. Atmospheric Chemistry and Physics. 18, 12933-12952. https://doi.org/10.5194/acp-18-12933-2018.

Liu, S., Yuan, J., 2020. Spatial and temporal variations of NO_2 density in Beijing-Tianjin-Hebei air pollution transmission path cities from 2006 to 2017. Earth and Environment. 48, 171-180. https://doi.org/10.14050/j.cnki.1672-9250.2020.48.035. (in Chinese).

Liu, T., Gong, S., He, J., Yu, M., Wang, Q., Li, H., Liu, W., Zhang, J., Li, L., Wang, X., Li, S., Lu, Y., Du, H., Wang, Y., Zhou, C., Liu, H., Zhao, Q., 2017b. Attributions of meteorological and emission factors to the 2015 winter severe haze pollution episodes in China's Jing-Jin-Ji area. Atmospheric Chemistry and Physics. 17, 2971-2980. https://doi.org/10.5194/acp-17-2971-2017.

Ma, T., Duan, F., He, K., Qin, Y., Tong, D., Geng, G., Liu, X., Li, H., Yang, S., Ye, S., Xu, B., Zhang, Q., Ma, Y., 2019. Air pollution characteristics and their relationship with emissions and meteorology in the Yangtze River Delta region during 2014–2016. Journal of Environmental Sciences. 83, 8-20. https://doi.org/10.1016/j.jes.2019.02.031.

Mao, S., Chen, G., Liu, F., Li, N., Wang, C., Liu, Y., Liu, S., Lu, Y., Xiang, H., Guo, Y., Li, S., 2020. Long-term effects of ambient air pollutants to blood lipids and dyslipidemias in a Chinese rural population. Environ. Pollut. 256, 113403. https://doi.org/10.1016/j.envpol.2019.113403.

Meng, K., Xu, X., Cheng, X., Xu, X., Qu, X., Zhu, W., Ma, C., Yang, Y., Zhao, Y., 2018. Spatio-temporal variations in SO_2 and NO_2 emissions caused by heating over the Beijing-Tianjin-Hebei Region constrained by an adaptive nudging method with OMI data. Sci. Total. Environ. 642, 543-552.

https://doi.org/10.1016/j.scitotenv.2018.06.021.

MEP, 2009. Ambient air-determiation of nitrogen oxides -N-(1-naphthyl) ethylene diamine dihydrochloride spectrophotometric method. The Ministry of Environmental Protection (MEP). Beijing, China. http://www.mee.gov.cn/ywgz/fgbz/bz/bzwb/jcffbz/200910/t20091010_162169.shtml. Accessed 3 November 2020.

MEP, 2012. Ambient air quality standards (GB 3095-2012). The Ministry of Environmental Protection (MEP). Beijing, China. http://kjs.mee.gov.cn/hjbhbz/bzwb/dqhjbh/dqhjzlbz/201203/t20120302_224165.htm. Accessed 3 November 2020.

MEP, 2013. Technical Regulation for Selection of Ambient Air Quality Monitoring Stations (on trial). The Ministry of Environmental Protection (MEP). Beijing, China. http://www.mee.gov.cn/ywgz/fgbz/bz/bzwb/jcffbz/201309/t20130925_260810.shtml. Accessed 3 November 2020.

MEP, 2018. Announcement on the issuance of the amendment to the ambient air quality standard (GB 3095-2012). The Ministry of Environmental Protection (MEP). Beijing, China. http://www.gov.cn/zwgk/2012-03/02/content_2081359.htm. Accessed 3 November 2020.

Prasad, A.K., Singh, R.P., Kafatos, M., 2012. Influence of coal-based thermal power plants on the spatial-temporal variability of tropospheric NO_2 column over India. Environ. Monit. Assess. 184, 1891-1907. https://doi.org/10.1007/s10661-011-2087-6.

Qu, Z., Henze, D.K., Capps, S.L., Wang, Y., Xu, X., Wang, J., Keller, M., 2017. Monthly top-down NO_x emissions for China (2005-2012): A hybrid inversion method and trend analysis. Journal of Geophysical Research: Atmospheres. 122, 4600-4625. https://doi.org/10.1002/2016jd025852.

SCPRC, 2018. Three-year plan on defending the blue sky. State Council of the People's

Republic of China (SCPRC). Beijing, China. http://www.gov.cn/zhengce/content/2018-07/03/content_5303158.htm?from=timeline. Accessed 3 November 2020.

Shen, Y., Zhang, L., Fang, X., Ji, H., Li, X., Zhao, Z., 2019. Spatiotemporal patterns of recent $PM_{2.5}$ concentrations over typical urban agglomerations in China. Sci Total Environ. 655, 13-26. https://doi.org/10.1016/j.scitotenv.2018.11.105.

Shi, K., Di, B., Zhang, K., Feng, C., Svirchev, L., 2018. Detrended cross-correlation analysis of urban traffic congestion and NO_2 concentrations in Chengdu. Transportation Research Part D: Transport and Environment. 61, 165-173. https://doi.org/10.1016/j.trd.2016.12.012.

Silvern, R.F., Jacob, D.J., Mickley, L.J., Sulprizio, M.P., Travis, K.R., Marais, E.A., Cohen, R.C., Laughner, J.L., Choi, S., Joiner, J., Lamsal, L.N., 2019. Using satellite observations of tropospheric NO_2 columns to infer long-term trends in US NO_x emissions: the importance of accounting for the free tropospheric NO_2 background. Atmospheric Chemistry and Physics. 19, 8863-8878. https://doi.org/10.5194/acp-19-8863-2019.

Skamarock, W.C., Klemp, Joseph B, Dudhia, Jimy, Gill, David, 2008. A description of the Advanced Research WRF Version 3, NCAR technical note, Mesoscale and Microscale Meteorology Division (National Center for Atmospheric Research, Boulder, CO, 2008). http://dx.doi.org/10.5065/D68S4MVH.

Sun, Y., Zhao, C., Su, Y., Ma, Z., Li, J., Letu, H., Yang, Y., Fan, H., 2019b. Distinct impacts of light and heavy precipitation on $PM_{2.5}$ mass concentration in Beijing. Earth and Space Science. 6, 1915-1925. https://doi.org/10.1029/2019ea000717.

Sun, Z., Yang, L., Bai, X., Du, W., Shen, G., Fei, J., Wang, Y., Chen, A., Chen, Y., Zhao, M., 2019a. Maternal ambient air pollution exposure with spatial-temporal variations and preterm birth risk assessment during 2013-2017 in Zhejiang Province, China. Environ. Int. 133, 105242. https://doi.org/10.1016/j.envint.2019.105242.

938 Tiwari, S., Dahiya, A., Kumar, N., 2015. Investigation into relationships among NO,
939 NO_2, NO_x, O_3, and CO at an urban background site in Delhi, India. Atmospheric
940 Research. 157, 119-126. https://doi.org/10.1016/j.atmosres.2015.01.008.
941 Vermeuel, M.P., Novak, G.A., Alwe, H.D., Hughes, D.D., Kaleel, R., Dickens, A.F.,
942 Kenski, D., Czarnetzki, A.C., Stone, E.A., Stanier, C.O., Pierce, R.B., Millet, D.B.,
943 Bertram, T.H., 2019. Sensitivity of ozone production to NO_x and VOC along the
944 Lake Michigan Coastline. Journal of Geophysical Research: Atmospheres. 124,
945 10989-11006. https://doi.org/10.1029/2019JD030842.
946 Wang, N., Lyu, X., Deng, X., Huang, X., Jiang, F., Ding, A., 2019. Aggravating O_3
947 pollution due to NO_x emission control in eastern China. Sci. Total. Environ. 677,
948 732-744. https://doi.org/10.1016/j.scitotenv.2019.04.388.
949 Wei, P., Ren, Z., Su, F., Cheng, S., Zhang, P., Gao, Q., 2012. Environmental process
950 and convergence belt of atmospheric NO_2 pollution in North China. Acta
951 Meteorologica Sinica. 25, 797-811. https://doi.org/10.1007/s13351-011-0610-x.
952 Wheeler, A.J., Smith-Doiron, M., Xu, X., Gilbert, N.L., Brook, J.R., 2008. Intra-urban
953 variability of air pollution in Windsor, Ontario—measurement and modeling for
954 human exposure assessment. Environ Res. 106, 7-16.
955 https://doi.org/10.1016/j.envres.2007.09.004.
956 Wu, R., Song, X., Chen, D., Zhong, L., Huang, X., Bai, Y., Hu, W., Ye, S., Xu, H., Feng,
957 B., Wang, T., Zhu, Y., Fang, J., Liu, S., Chen, J., Wang, X., Zhang, Y., Huang, W.,
958 2019. Health benefit of air quality improvement in Guangzhou, China: Results
959 from a long time-series analysis (2006–2016). Environ Int. 126, 552-559.
960 https://doi.org/10.1016/j.envint.2019.02.064.
961 Xie, J., Liao, Z., Fang, X., Xu, X., Wang, Y., Zhang, Y., Liu, J., Fan, S., Wang, B., 2019.
962 The characteristics of hourly wind field and its impacts on air quality in the Pearl
963 River Delta region during 2013–2017. Atmospheric Research. 227, 112-124.
964 https://doi.org/10.1016/j.atmosres.2019.04.023.
965 Xie, Y., Wang, W., Wang, Q., 2018. Spatial distribution and temporal trend of

tropospheric NO_2 over the Wanjiang City Belt of China. Advances in Meteorology. 2018, 1-13. https://doi.org/10.1155/2018/6597186.

Xie, Z., Du, Y., Zeng, Y., Li, Y., Yan, M., Jiao, S., 2009. Effects of precipitation variation on severe acid rain in southern China. Journal of Geographical Sciences. 19, 489-501. https://doi.org/10.1007/s11442-009-0489-y.

Xu, M., Sbihi, H., Pan, X., Brauer, M., 2019a. Local variation of $PM_{2.5}$ and NO_2 concentrations within metropolitan Beijing. Atmos Environ. 200, 254-263. https://doi.org/10.1016/j.atmosenv.2018.12.014.

Xu, Y., Xue, W., Lei, Y., 2019b. Impact of meteorological conditions and emission change on $PM_{2.5}$ pollution in China. China Environ Sci. 39, 4546-4551. https://doi.org/10.19674/j.cnki.issn1000-6923.2019.0529. (in Chinese).

Xu, Y., Xue, W., Lei, Y., Huang, Q., Zhao, Y., Cheng, S., Ren, Z., Wang, J., 2020. Spatiotemporal variation in the impact of meteorological conditions on $PM_{2.5}$ pollution in China from 2000 to 2017. Atmospheric Environment. 223, 117215. https://doi.org/10.1016/j.atmosenv.2019.117215.

Yan, D., Lei, Y.L., Shi, Y.K., Zhu, Q., Li, L., Zhang, Z.E., 2018. Evolution of the spatiotemporal pattern of $PM_{2.5}$ concentrations in China – A case study from the Beijing-Tianjin-Hebei region. Atmos Environ. 183, 225-233. https://doi.org/10.1016/j.atmosenv.2018.03.041.

Yang, J., Ji, Z., Kang, S., Zhang, Q., Chen, X., Lee, S.Y., 2019. Spatiotemporal variations of air pollutants in western China and their relationship to meteorological factors and emission sources. Environ. Pollut. 254, 112952. https://doi.org/10.1016/j.envpol.2019.07.120.

Yang, J., Kang, S., Ji, Z., Yin, X., Tripathee, L., 2020. Investigating air pollutant concentrations, impact factors, and emission control strategies in western China by using a regional climate-chemistry model. Chemosphere. 246, 125767. https://doi.org/10.1016/j.chemosphere.2019.125767.

Yang, X., Zhao, C., Guo, J., Wang, Y., 2016. Intensification of aerosol pollution

associated with its feedback with surface solar radiation and winds in Beijing. Journal of Geophysical Research: Atmospheres. 121, 4093-4099. https://doi.org/10.1002/2015jd024645.

Yang, Y., Wang, K., Cui, C., Liu, Y., Huang, L., 2015. Analysis of relationship between air pollution and meteorological conditions of Harbin. Chinese Journal of Environmental Engineering. 9, 5945-5950. (in Chinese).

Zhang, H., Wang, Y., Hu, J., Ying, Q., Hu, X.M., 2015. Relationships between meteorological parameters and criteria air pollutants in three megacities in China. Environ. Res. 140, 242-254. https://doi.org/10.1016/j.envres.2015.04.004.

Zhang, K., Zhao, C., Fan, H., Yang, Y., Sun, Y., 2019b. Toward understanding the differences of $PM_{2.5}$ characteristics among five China urban cities. Asia-Pacific Journal of Atmospheric Sciences. 56, 493-502. https://doi.org/10.1007/s13143-019-00125-w.

Zhang, L., Lee, C.S., Zhang, R., Chen, L., 2017. Spatial and temporal evaluation of long term trend (2005–2014) of OMI retrieved NO_2 and SO_2 concentrations in Henan Province, China. Atmos Environ. 154, 151-166. https://doi.org/10.1016/j.atmosenv.2016.11.067.

Zhang, Q., Geng, G., 2019. Impact of clean air action on $PM_{2.5}$ pollution in China. Science China Earth Sciences. 62, 1845-1846. https://doi.org/10.1007/s11430-019-9531-4.

Zhang, Q., Zheng, Y., Tong, D., Shao, M., Wang, S., Zhang, Y., Xu, X., Wang, J., He, H., Liu, W., Ding, Y., Lei, Y., Li, J., Wang, Z., Zhang, X., Wang, Y., Cheng, J., Liu, Y., Shi, Q., Yan, L., Geng, G., Hong, C., Li, M., Liu, F., Zheng, B., Cao, J., Ding, A., Gao, J., Fu, Q., Huo, J., Liu, B., Liu, Z., Yang, F., He, K., Hao, J., 2019a. Drivers of improved $PM_{2.5}$ air quality in China from 2013 to 2017. Proc. Natl. Acad. Sci. U. S. A. 116, 24463-24469. https://doi.org/10.1073/pnas.1907956116.

Zhang, X., Xu, X., Ding, Y., Liu, Y., Zhang, H., Wang, Y., Zhong, J., 2019c. The impact of meteorological changes from 2013 to 2017 on $PM_{2.5}$ mass reduction in key

regions in China. Science China Earth Sciences. 62, 1885-1902. https://doi.org/10.1007/s11430-019-9343-3.

Zhao, C., Andrews, A.E., Bianco, L., Eluszkiewicz, J., Hirsch, A., MacDonald, C., Nehrkorn, T., Fischer, M.L., 2009. Atmospheric inverse estimates of methane emissions from Central California. Journal of Geophysical Research. 114. https://doi.org/10.1029/2008jd011671.

Zhao, C., Wang, Y., Shi, X., Zhang, D., Wang, C., Jiang, J.H., Zhang, Q., Fan, H., 2019. Estimating the contribution of local primary emissions to particulate pollution using high-density station observations. Journal of Geophysical Research: Atmospheres. 124, 1648-1661. https://doi.org/10.1029/2018jd028888.

Zhao, S., Hu, B., Gao, W., Li, L., Huang, W., Wang, L., Yang, Y., Liu, J., Li, J., Ji, D., Zhang, R., Zhang, Y., Wang, Y., 2020. Effect of the “coal to gas” project on atmospheric NO_x during the heating period at a suburban site between Beijing and Tianjin. Atmospheric Research. 241, 104977. https://doi.org/10.1016/j.atmosres.2020.104977.

Zhao, S., Yu, Y., Yin, D., Qin, D., He, J., Dong, L., 2018. Spatial patterns and temporal variations of six criteria air pollutants during 2015 to 2017 in the city clusters of Sichuan Basin, China. Sci. Total. Environ. 624, 540-557. https://doi.org/10.1016/j.scitotenv.2017.12.172.

Zhao, W., Shu, Z., 2019. Spatial and temporal evolution of urban economic linkages in Shandong Peninsula urban agglomeration. Journal of Ludong University (Natural Science Edition). 35, 346-351. (in Chinese).

Zheng, B., Tong, D., Li, M., Liu, F., Hong, C., Geng, G., Li, H., Li, X., Peng, L., Qi, J., Yan, L., Zhang, Y., Zhao, H., Zheng, Y., He, K., Zhang, Q., 2018b. Trends in China's anthropogenic emissions since 2010 as the consequence of clean air actions. Atmos. Chem. Phys. 18, 14095-14111. https://doi.org/10.5194/acp-18-14095-2018.

Zheng, C., Zhao, C., Li, Y., Wu, X., Zhang, K., Gao, J., Qiao, Q., Ren, Y., Zhang, X.,

Chai, F., 2018a. Spatial and temporal distribution of NO_2 and SO_2 in Inner Mongolia urban agglomeration obtained from satellite remote sensing and ground observations. Atmospheric Environment. 188, 50-59. https://doi.org/10.1016/j.atmosenv.2018.06.029.

Zheng, C., Zhao, C., Zhu, Y., Wang, Y., Shi, X., Wu, X., Chen, T., Wu, F., Qiu, Y., 2017. Analysis of influential factors for the relationship between $PM_{2.5}$ and AOD in Beijing. Atmospheric Chemistry and Physics. 17, 13473-13489. https://doi.org/10.5194/acp-17-13473-2017.

Zhong, Z., Zheng, J., Zhu, M., Huang, Z., Zhang, Z., Jia, G., Wang, X., Bian, Y., Wang, Y., Li, N., 2018. Recent developments of anthropogenic air pollutant emission inventories in Guangdong province, China. Sci. Total. Environ. 627, 1080-1092. https://doi.org/10.1016/j.scitotenv.2018.01.268.

Zhou, X., Zhang, T., Li, Z., Tao, Y., Wang, F., Zhang, X., Xu, C., Ma, S., Huang, J., 2018. Particulate and gaseous pollutants in a petrochemical industrialized valley city, Western China during 2013–2016. Environmental Science and Pollution Research. 25, 15174-15190. https://doi.org/10.1007/s11356-018-1670-6.

Supplementary Materials for

Impact of weather and emission changes on NO_2 concentrations in China during 2014−2019

Yang Shen [a], Fei Jiang [a,b*], Shuzhuang Feng [a], Yanhua Zheng [a], Zhe Cai [c], Xiaopu Lyu [d]

[a] *Jiangsu Provincial Key Laboratory of Geographic Information Science and Technology, International Institute for Earth System Science, Nanjing University, Nanjing, 210023, China*

[b] *Jiangsu Center for Collaborative Innovation in Geographical Information Resource Development and Application, Nanjing, 210023, China*

[c] *Nanjing Climblue Technology co., LTD, Nanjing, Jiangsu 211135, China*

[d] *Department of Civil and Environmental Engineering, Hong Kong Polytechnic University, Hong Kong*

* Corresponding author

E-mail address: jiangf@nju.edu.cn; Tel.: +86-25-83597077; Fax: +86-25-83592288;

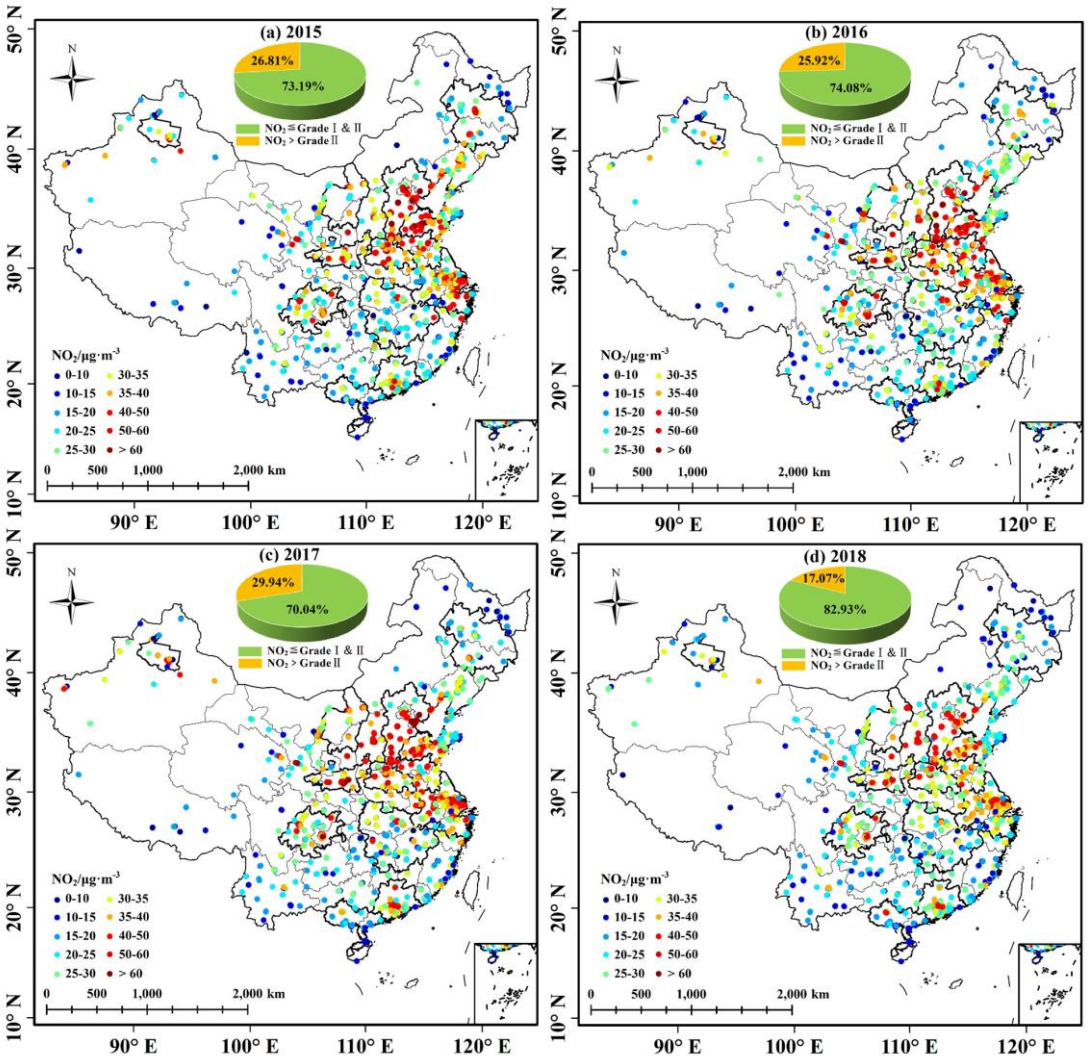

Figure S1. Spatial distribution of annual surface average NO_2 concentrations in China for (a) 2015, (b) 2016, (c) 2017, and (d) 2018. Pie charts give the percentage of stations exhibiting annual mean NO_2 concentrations within the Chinese Ambient Air Quality Standards (CAAQS) Grade I and II annual standards for each year. The sites with the annual averaged concentration of NO_2 below the CAAQS Grade II annual standard (40 $\mu g \cdot m^{-3}$) account for more than 70% from 2015 to 2017 and exceed 80% in 2018.

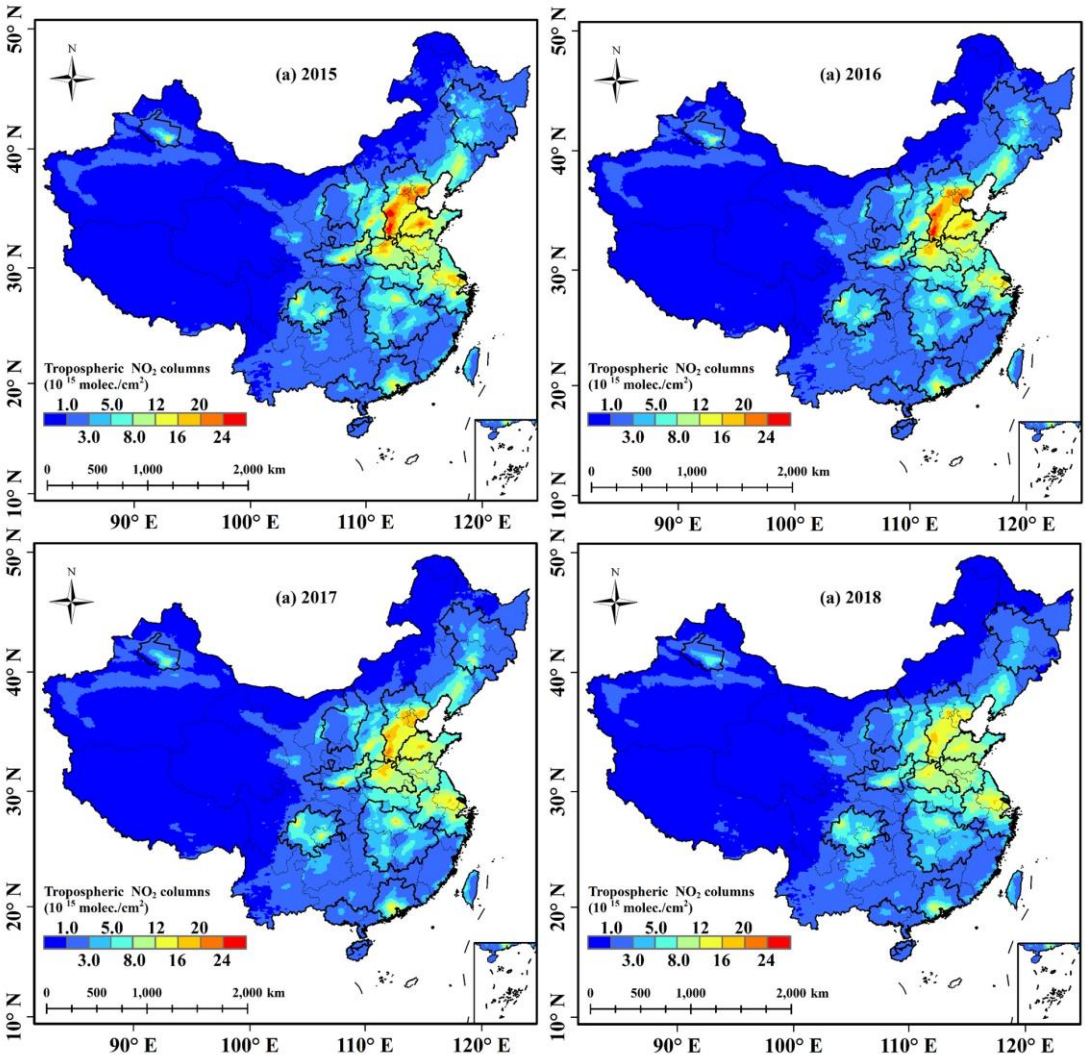

Figure S2. Spatial distribution of annual averaged OMI-retrieved NO_2 columns in China for (a) 2015, (b) 2016, (c) 2017, and (d) 2018.

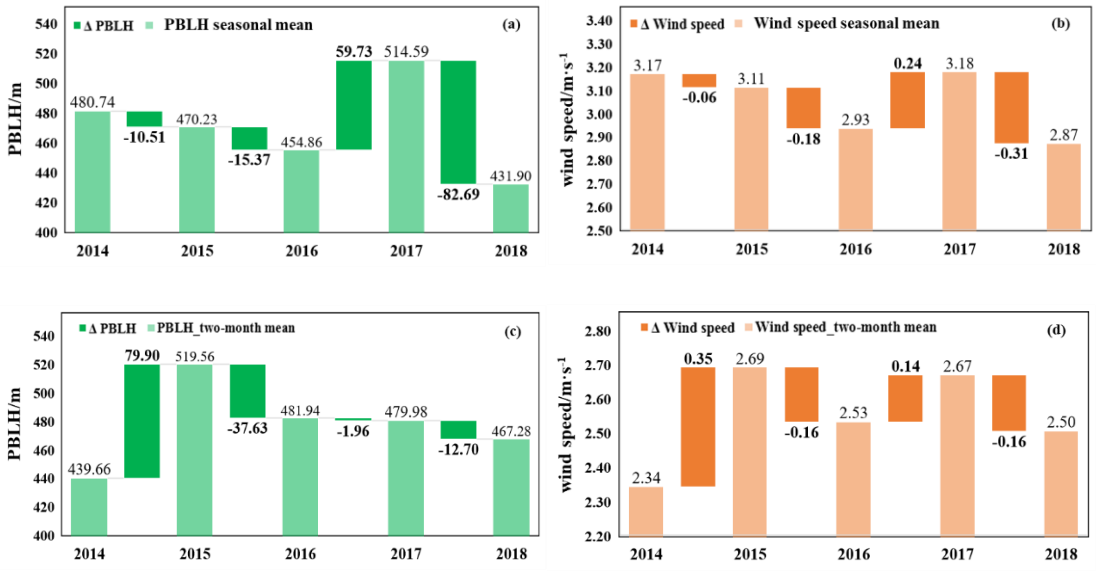

Figure S3. (a) The average planetary boundary layer height (PBLH) and interannual variations of PBLH in winter from 2014 to 2018 in BTH; (b) The same as (a), but for wind speed. (c) and (d) are the same as (a) and (b), respectively, but for the summer of PRD. ERA-Interim reanalysis monthly mean data (PBLH and wind speed data at 10 m) were acquired from the European Center for Medium−Range Weather Forecasts (ECMWF).

List of Tables

Table S1. Number of air quality monitoring sites selected in typical urban agglomerations and the whole country from June 2014 to May 2019

Urban Agglomeration	The number of sites per year					
	2014	2015	2016	2017	2018	2019
BTH	83	84	87	87	88	85
YRD	115	135	148	143	147	149
YRMR	70	148	151	152	150	150
CY	52	88	91	92	90	89
PRD	73	73	72	73	75	74
HC	44	56	55	55	57	56
CS	39	54	54	55	58	57
CP	28	58	58	59	66	62
SP	59	58	56	63	60	62
NSTM	11	17	4	12	17	17
BG	30	41	41	41	41	41
HBEY	19	23	23	23	25	24

Table S2. Research time range and the division of seasons in this study

Year	Seasons			
	Spring	Summer	Autumn	Winter
2014	/	Jun., Jul., Aug.	Sep., Oct., Nov.	Dec., Jan., Feb.
2015	Mar. Apr., May.	Jun., Jul., Aug.	Sep., Oct., Nov.	Dec., Jan., Feb.
2016	Mar. Apr., May.	Jun., Jul., Aug.	Sep., Oct., Nov.	Dec., Jan., Feb.
2017	Mar. Apr., May.	Jun., Jul., Aug.	Sep., Oct., Nov.	Dec., Jan., Feb.
2018	Mar. Apr., May.	Jun., Jul., Aug.	Sep., Oct., Nov.	Dec., Jan., Feb.
2019	Mar. Apr., May.	/	/	/

1113